Bioelectrochemistry 164 (2025) 108940

Contents lists available at ScienceDirect

Bioelectrochemistry

journal homepage: www.journals.elsevier.com/bioelectrochemistry

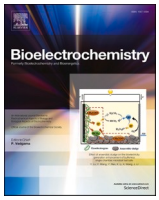

Bystander effect of metal byproducts released from electroporated cells after electroporation *in vitro*

Alenka Maček Lebar [a,*], Tjaša Potočnik [a], Janez Ščančar [b], Stefan Marković [b], Tamara Polajžer [a]

[a] University of Ljubljana, Faculty of Electrical Engineering, Tržaška 25 1000 Ljubljana, Slovenia
[b] Jožef Stefan Institute, Department of Environmental Sciences, Jamova cesta 39 1000 Ljubljana, Slovenia

ARTICLE INFO

Keywords:
Pulsed electric fields
Stainless-steel electrodes
Aluminum cuvettes
Electrode dissolution

ABSTRACT

Electrodes dissolution during electroporation releases metal ions into the medium, altering the microenvironment of electroporated cells and allowing metal ions to penetrate cell membrane. During cell membrane repair, homeostasis restoration or activation of cell death pathways, cells eliminate excess metals from the cytoplasm and membrane. This study assessed the effects of post-electroporation metal byproducts on untreated (non-electroporated) cells *in vitro*.

CHO and HCT116 cells were electroporated with three pulse protocols (unipolar: 100 μs, 5 ms; bipolar: 2 μs) using either aluminum or stainless-steel electrodes. After electroporation, cells were transferred to fresh growth medium and incubated for 2 or 4 h. Incubation period allowed either cell recovery or the activation of cell death pathways, leading to the accumulation of metal byproducts in the incubation medium.

Stainless-steel electrodes with the 5 ms pulse protocol caused a considerable increase in iron, chromium and nickel ions in incubation medium compared to aluminum electrodes or other protocols. Metal ions in incubation medium caused toxicity in non-electroporated cells, disrupting cell cycle function or inducing cell death. The observed toxicity results from combined effects of metal ions on cellular functions and the mechanisms the cells use to protect themselves from metal overload.

1. Introduction

Exposure of biological cells to short electric pulses leads to structural and chemical changes in the plasma membrane [1]. These changes lead to a transient increase in membrane permeability. Based on the accepted theory that initially small aqueous pores form in the lipid bilayer of the cell membrane, the phenomenon was named electroporation [2]. Electroporation has a widespread use in many medical and biotechnological applications as well as in the food industry [3,4,5,6,7,8,9]. In order to introduce nucleic acids and chemotherapeutic drugs into cells, the cells have to remain viable after exposure to electric field, meaning that electroporation must be reversible. For ablation of tissue (tumors and heart muscle), an irreversible type of electroporation that leads to cell death is needed. The (i)reversibility of electroporation depends on the parameters of the electric pulse protocol (amplitude, duration, polarity, etc.) to which the cells are exposed, but also vary from cell to cell and depend on incubation/recovery medium and temperature when performed *in vitro* [1].

The cells are usually exposed to an electric field via metal electrodes through which high voltage electric pulses are delivered. Electrochemical reactions take place at the interface between the electrode and electrolyte, causing electrolysis. Electrolysis leads to the release of metal ions from the electrodes, pH changes, dehydration due to electroosmotic pressure, secondary chemical reactions and the formation of new chemical species, the formation of radicals and gases such as oxygen, hydrogen and chlorine in form of bubbles [10,11,12]. The intensity of chemical reactions and the amount of electrolytic products depend on electric pulse parameters (duration, amplitude, polarity, etc.) [12,13,14]. Previous studies have shown that the products of electrolysis can contribute to cell death under *in vitro* and *in vivo* conditions [10,11,15,16,17,18,19], precipitate proteins and nucleic acids [20] and have an impact on treated food [21]. Particular attention was given to the potential beneficial effects of electrolytic products and pH changes contributing to tumor ablation [10] and the potential risk of bubble formation in intracardiac pulsed field ablation [22]. Over the past decade, the effectiveness of electrolytic ablation—an electrochemical treatment that uses low-voltage direct current to ablate tissue [23]—has been enhanced by combining it with high-voltage pulses. These pulses

* Corresponding author.
E-mail address: alenka.macek.lebar@fe.uni-lj.si (A.M. Lebar).

https://doi.org/10.1016/j.bioelechem.2025.108940
Received 25 November 2024; Received in revised form 21 January 2025; Accepted 7 February 2025
Available online 12 February 2025

cause electroporation, and the combined technique is known as electrolytic electroporation [24]. The use of exponentially decaying electric pulses [25] or a combination of a few short high-voltage pulses and larger number of longer low-voltage pulses [26] has been proposed to achieve large ablation volumes. The initial high-voltage spike(s) induces electroporation, and the subsequent low-voltage tail has an electrolytic and electrophoretic effect. This approach produces a synergistic effect that enhances the effect of electroporation and electrolytic ablation, thereby increasing the ablated area and shortening the treatment time [24,27,28]. The working hypothesis of the method is that reversible electroporation of the cell membranes enables the electrolysis products to enter the cells in high concentrations and induce cell death, similar to electrochemotherapy (ECT) [28].

Dissolution of the electrodes is one of the basic electrolytic reactions during electric pulses delivery. Metal ions released from electrodes can drastically change the microenvironment of the cells. Although several transition metals, such as zinc, iron (Fe), copper (Cu), cobalt and manganese participate in the control of cell metabolic and signaling pathways, their redox properties give them ability to produce reactive radicals and generate reactive oxygen species (ROS) and reactive nitrogen species (RNS). These free radicals cause modifications to DNA bases, enhance lipid peroxidation, and alter calcium and sulfhydryl homeostasis. Lipid peroxides, formed by the attack of radicals on polyunsaturated fatty acid residues of phospholipids, can further react with redox metals finally producing mutagenic and carcinogenic products [29].

Stainless-steel (SS) electrodes and aluminum (Al) cuvettes are most often used for electroporation experiments *in vitro*. Aluminum cuvettes are widely utilized due to their availability and cost-effectiveness. While aluminum cuvettes are generally used only once, SS electrodes are intended for multiple uses. However, repeated use can alter the surface properties of the electrodes. Studies have shown that using an Al cathode results in a greater pH change of electroporation medium compared to platinum, copper, or SS cathodes, especially in high conductive media [30]. Metal ions released from electrodes interact with biological macromolecules, like DNA, RNA and proteins, and cause their precipitation. It has been reported that Al electrodes cause greater precipitation than SS electrodes [20]. Furthermore, during the application of electric pulses lasting several tens of milliseconds, large aggregates of Al hydroxide may form. These aggregates have been shown to interact with recombinant adenovirus particles, forming virus-metallic aggregate complexes that can then efficiently enter cells through one or more endocytosis processes [31]. Furthermore, the Al ions released from Al electrodes were found to be less toxic than the Fe ions released from SS electrodes at the same pulse parameters. Fe ions, released from the electrodes, have been shown to significantly impair cell viability [13,19]. Fe, of course, is the main component of stainless steels, therefore the high amount of released Fe ions from SS electrodes has been identified as a key factor of cytotoxicity [15,19]. A comparison of metal ion release from platinum, Al, and SS electrodes revealed significantly higher concentrations of Al released from Al electrodes and Fe and nickel (Ni) from SS electrodes after treatment with 8 × 100 μs monophasic pulses delivered at frequency 1 Hz than with high-frequency bipolar pulses (HF-BP) or nanosecond pulses. These studies also demonstrated that the duration of electroporation pulses greatly affects the amount of metal ions released during electroporation [14,32].

The electrolysis products near electroporated cells can easily attach to cell membrane or penetrate cell membrane, thus entering the cell. Even after membrane integrity is restored, the cell must actively remove undesirable components from both the cytoplasm and the membrane to reestablish homeostasis. These processes can continue for hours following electroporation. The accumulation of secreted byproducts in the surrounding environment may affect nearby untreated cells, leading to a phenomenon known as the bystander effect. Recent studies [33,34] have shown that excess Fe can be secreted through extracellular vesicles (EVs), and the uptake of these EVs may induce oxidative damage in recipient cells. Moreover, Fe and lipid peroxidation are both required for ferroptosis, which in the case of cell lysis is spreading through cell populations in a lipid peroxide and Fe-dependent manner [35,36]. The potential for dying cells to release EVs capable of affecting target cells or tissues is also of significant interest [37,38].

Electrode dissolution during electroporation leads to the formation of metal ions, while post-electroporation metal byproducts are formed after electroporation, during the recovery of damaged cell membrane, restoration of homeostasis or initiation of cell death pathways. Post-electroporation metal byproducts are released into the cell surroundings minutes to hours after electroporation. This study aimed to evaluate the effects of post-electroporation metal byproducts on untreated (i.e. non-electroporated) cells *in vitro*, using two cell lines, Al and SS electrodes and three distinct pulse protocols.

2. Materials and Methods

2.1. Cells

Chinese hamster ovary cell line (CHO-K1; European Collection of Cell Cultures, UK) and human colorectal carcinoma cell line (HCT116; ATCC, CCL-247) were used in experiments. Cells were grown in 150 mm^2 culture flasks (TPP, Switzerland) for 2–4 days in an incubator (Kambič, Slovenia) at 37° C, in a humid atmosphere of 5 % CO_2 in air until 70–80 % confluency was reached. CHO cells were cultured in HAM-F12 growth medium (PAA, Austria) supplemented with 10 % fetal bovine serum (Sigma Aldrich, Germany), L-glutamine (StemCell, Canada) and antibiotics penicillin/streptomycin (PAA, Austria), and gentamycin (Sigma Aldrich, Germany). HCT116 cells were cultured in Dulbecco's modified Eagle's Medium (DMEM) growth medium (Sigma Aldrich, Germany) supplemented with 10 % fetal bovine serum (Sigma Aldrich, Germany), L-glutamine (StemCell, Canada) and antibiotics penicillin/streptomycin (PAA, Austria), and gentamycin (Sigma Aldrich, Germany).

For experiments, growth medium was removed and the trypsin-EDTA (5 g trypsin/2 g EDTA in 0.9 % NaCl; Sigma-Aldrich, Germany) 10 × diluted in Hanks' Balanced Salt solution (Sigma-Aldrich, Germany) was added to detach cells. From the obtained cell suspension, trypsin and growth medium were removed by centrifugation at 180 g for 5 min at room temperature (Sigma 3–15 K, UK). The cell pellet was then resuspended in HAM-F12 growth medium for CHO-K1 cell line or DMEM growth medium for HCT116 cell line to obtain a final cell density of 1 × 10^7 cells/ml.

2.2. Electric pulses delivery

Cells were exposed to a train of eight monopolar rectangular pulses of 100 μs duration with a repetition frequency of 1 Hz (electric fields 0–2 kV/cm), to a train of eight monopolar rectangular pulses of 5 ms duration with a repetition frequency of 1 Hz (electric fields 0–0.875 kV/cm), or to a high frequency bipolar pulses (HF-BP) (electric fields 0–2 kV/cm). In HF-BP protocol bipolar pulses of 2 μs duration of positive and negative phase were applied. The pause between positive and negative pulse phase and pause between bipolar pulses were 2 μs. 50 bursts were applied and in each burst 50 pulses were delivered. Burst repetition rate was 1 Hz. All pulses were delivered with a laboratory prototype pulse generator (University of Ljubljana), based on H-bridge digital amplifier with 1 kV MOSFETs (DE275-102N06A, IXYS, USA). Pulse delivery was monitored by the oscilloscope WaveSurfer 422, 200 MHz with high voltage differential voltage probe ADP305 and current probe CP030 (Teledyne LeCroy, USA).

2.3. Electrodes

Two types of electrodes were used in this study: custom plate stainless 304 steel electrodes and commercially available aluminum

electroporation cuvettes (VWR International, USA). Both electrodes have the same geometry and distance between the electrodes (4 mm). During electric pulses delivery all the cells were exposed to approximately the same electric field, which was estimated as voltage applied divided by the distance between the electrodes.

2.4. Permeabilization

Cell membrane permeabilization of CHO and HCT116 cells in suspension was determined as percentage of propidium iodide (PI) fluorescent cells. 5 μl of PI (100 μg/ml), (Life Technologies, USA), was added to 200 μl of cells in growth medium at concentration 1×10^7 cells/ml in electroporation cuvette with 4 mm gap (VWR International, USA) before pulse delivery. Emission of PI fluorescence was detected by flow cytometry (Attune NxT, USA) using a blue laser excitation at 488 nm and detecting the emitted fluorescence through a 574/26 nm band-pass filter, 5 min after exposure of cells to electric pulses. At every measurement 10,000 events were recorded. Data obtained were analyzed with the Attune NxT software (version 3.1.2).

2.5. Cell survival after electroporation

For cell survival experiments, 200 μl of cells in suspension in growth medium at concentration 1×10^7 cells/ml was pipetted in a 4 mm gap electroporation cuvette (VWR International, USA). After pulse application cells were incubated for 5 min at room temperature, afterwards 2×10^4 CHO or 5×10^4 HCT116 cells from cuvette were seeded in 100 μl of growth medium in 96 well plate (TPP, Switzerland). Cells were seeded in triplicates. The plate was then incubated 24 h (37 °C, 5 % CO_2). Cell survival was determined with the MTS-based Cell Titer 96 AQueous One Solution Cell Proliferation Assay (Promega, USA). After incubation 20 μl of MTS reagent were added to each well and cells were incubated for additional 2 h in the incubator (37 °C, 5 % CO_2). Absorption at 490 nm wavelength was measured with a Tecan Infinite M200 spectrophotometer (Tecan, Switzerland). To calculate the percentage of viable cells the absorption of each cell sample was divided by an average absorption of the control cell samples, in which cells were treated as described but not exposed to electric pulses.

2.6. Incubation medium preparation

When SS electrodes were used, a drop of prepared cell suspension (100 μl, 10^6 cells) was pipetted between the electrodes. For pulse delivery the electrodes were positioned vertically on the bottom of the petri dish. Afterwards the electrodes were removed and a drop of electroporated cell suspension was incubated for 5 min at room temperature to allow cell recovery. The electrodes were cleaned with ethanol (Lekarna Ljubljana, Slovenia) and wiped with sterile cotton gauze after each exposure of the cells to electric pulses. When Al electrodes were used, 200 μl (2×10^6 cells) of prepared cell suspension was pipetted in new electroporation cuvette. After delivery of the pulses, the electroporated cell suspension was left inside the electroporation cuvette for 5 min at room temperature to allow cell recovery.

To obtain a sufficient volume of the sample needed for analysis four electroporated samples from SS electrodes, and two samples from Al cuvettes (both total 4×10^6 cells) were collected in a microcentrifuge tube. The electroporated medium was collected by centrifugation at 180 g for 5 min at room temperature (Sigma 3–15 K, UK). It was filtered with a syringe filter with a pore size of 0.8 μm (Acrodisc™ syringe filter with Supor™ membrane, VWR International, USA) to remove larger particles, cell debris and dead/floating cells, and subsequently used for further analysis of metal ion concentrations. The cell pellet was resuspended in 1 ml of fresh growth medium and incubated in an incubator (37 °C, 5 % CO_2) for 2 h or 4 h. After incubation, the incubation medium was separated from the cells by centrifugation at 180 g for 5 min at room temperature (Sigma 3–15 K, UK), carefully collected and filtered with a syringe filter with a pore size of 0.8 μm (Acrodisc™ syringe filter with Supor™ membrane, VWR International, USA) to exclude larger particles, cell debris and dead/floating cells. In this way approximately 700 μl of incubation medium was obtained from each sample (Scheme 1).

Short protocol descriptions for incubation medium preparation and short names of all incubation media used in the study are gathered in Table 1.

2.7. Cell survival in incubation medium

300 μl of incubation medium was transferred in each well of 96 well plate (TPP, Switzerland). Non-electroporated CHO cells (2×10^3) were seeded in incubation medium derived from electroporated CHO cells. Similarly, non-electroporated HCT116 cells (8×10^3) were seeded in incubation medium obtained from electroporated HCT116 cells. The amount of incubation medium was sufficient to seed two samples. The cells were grown in incubation medium (37 °C, 5 % CO_2) for 72 h. Cell survival was determined with the MTS assay as described in 2.5 (Scheme 2).

2.8. Exchange of incubation medium with growth medium

After non-electroporated CHO cells were grown in SS, 8 × 5 ms, 2 h incubation medium for 72 h, the incubation medium was removed from wells and replaced with 300 μl of fresh growth medium. The CHO cells were then left to grow for additional 72 h. Cell survival was determined with MTS as described in 2.5 (Scheme 2). For control, non-electroporated CHO cells were seeded in SS, 8 × 5 ms, 2 h incubation medium obtained at electric field of 0 kV/cm.

2.9. Mitochondrial membrane potential (MMP) assay

MMP was detected with the MitoProbe DiIC1(5) Assay Kit (M34151, Invitrogen, Thermo Fisher, USA).

$DiIC_1(5)$ penetrates the cytosol of eukaryotic cells and accumulates primarily in mitochondria with active MMP, producing bright, far-red fluorescence. Changes in MMP were detected with flow cytometer (Attune NxT, USA) using 637 nm red laser and 670/14 nm band-pass filter. The number of events analyzed was set at 10,000, but in the samples with low cell viability a lower number of events was detected (the smallest: 1000). On the dot-plots of forward-scatter and side-scatter, the debris and clusters were excluded from the analysis. Fluorescence intensity histograms were used to determine the changes in MMP signal. Data on median fluorescence of MMP signal for each sample were collected. Carbonyl cyanide m-chlorophenyl hydrazone (CCCP) was used as a positive control. CCCP is a MMP disrupter, resulting in decreased MMP and fluorescence.

CHO cells grown in SS, 8 × 5 ms, 2 h incubation medium for 72 h, were analyzed. The incubation medium was carefully removed from the wells of the 96-well plate. The cells in each well were trypsinized with 40 μl of trypsin solution. When the cells detached, 50 μl growth medium was added. The cell suspension from 4 wells was collected to obtain as many cells as possible in a 1.5 ml microcentrifuge tube and centrifuged at 180 g for 5 min. Meanwhile, the dye was prepared. 2 μl DiIC1(5) was added to 1 ml of fresh growth medium. The cell pellet was resuspended in 150 μl of the dye suspension and incubated at 37 °C for 20 min. The samples were then analyzed on flow cytometer (Scheme 2). The median value of the MMP fluorescence intensity of the samples was normalized to the median value of the MMP fluorescence intensity of the control samples (cells, grown in incubation medium obtained at electric field of 0 kV/cm). For the MMP-positive control, 150 μl of prepared CCCP solution (10 μl of the CCCP stock solution in 1 ml growth medium) was added to the cells stained with DiIC1(5), incubated for 5 min in the incubator, and analyzed on flow cytometer.

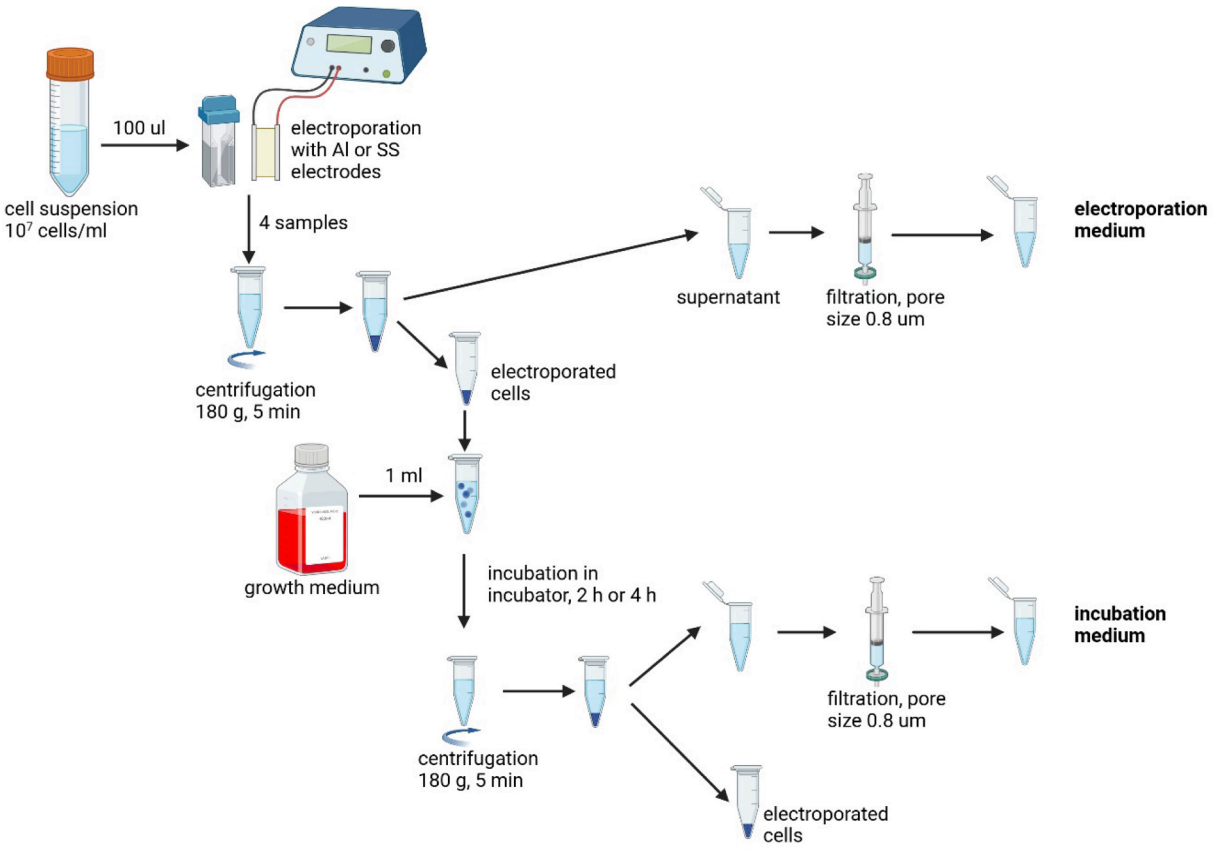

Scheme 1. Schematic representation of incubation medium preparation. Created in https://BioRender.com.

Table 1
Protocol descriptions for incubation medium preparation and their short names.

Protocol description for incubation medium preparation	Short name
Cells electroporated using aluminum electrodes and 8 × 100 μs pulse protocol incubated in growth medium for 2 h	Al, 8 × 100 μs, 2 h
Cells electroporated using aluminum electrodes and 8 × 100 μs pulse protocol incubated in growth medium for 4 h	Al, 8 × 100 μs, 4 h
Cells electroporated using aluminum electrodes and 8 × 5 ms pulse protocol incubated in growth medium for 2 h	Al, 8 × 5 ms, 2 h
Cells electroporated with aluminum electrodes and 8 × 5 ms pulse protocol incubated in growth medium for 4 h	Al, 8 × 5 ms, 4 h
Cells electroporated using aluminum electrodes and HV-BP pulse protocol and incubated in growth medium for 2 h	Al, HV-BP, 2 h
Cells electroporated using aluminum electrodes and HV-BP pulse protocol incubated in growth medium for 4 h	Al, HV-BP, 4 h
Cells electroporated using stainless-steel electrodes and 8 × 100 μs pulse protocol incubated in growth medium for 2 h	SS, 8 × 100 μs, 2 h
Cells electroporated using stainless-steel electrodes and 8 × 100 μs pulse protocol incubated in growth medium for 4 h	SS, 8 × 100 μs, 4 h
Cells electroporated using stainless-steel electrodes and 8 × 5 ms pulse protocol incubated in growth medium for 2 h	SS, 8 × 5 ms, 2 h
Cells electroporated using stainless-steel electrodes and 8 × 5 ms pulse protocol incubated in growth medium for 4 h	SS, 8 × 5 ms, 4 h
Cells electroporated using stainless-steel electrodes and HV-BP pulse protocol incubated in growth medium for 2 h	SS, HV-BP, 2 h
Cells electroporated using stainless-steel electrodes and HV-BP pulse protocol incubated in growth medium for 4 h	SS, HV-BP, 4 h

2.10. Cell cycle analysis

Cell cycle analysis was done with Hoechst 33342 dye (Thermo Fisher, USA) using flow cytometer (Attune NxT) equipped with 355 nm laser and 450/50 nm band-pass filter (Scheme 2). The number of events analyzed was set at 10,000, but in the samples with low cell viability lower number of events was detected (the smallest: 3000). On the dot-plots of forward-scatter and side-scatter, the debris and clusters were excluded from the analysis. On the dot-plots of area and width parameters for the DNA channel doublets were eliminated. Fluorescence intensity histograms were used to determine the number of events corresponding to cell cycle phases.

CHO cells grown in SS, 8 × 5 ms, 2 h incubation medium for 72 h, were analyzed. The incubation medium was carefully removed from the wells of the 96-well plate. The cells in each well were trypsinized with 40 μl of trypsin solution. When the cells detached, 50 μl growth medium was added. The cell suspension from 4 wells was collected in a 1.5 ml microcentrifuge tube to obtain as many cells as possible and centrifuged at 180 g for 5 min. Meanwhile, the dye was prepared. 2.5 μl Hoechst 33342 was added to 1 ml of fresh growth medium. The cell pellet was resuspended in 150 μl of the dye suspension and incubated at 37 °C for 1 h. The samples were then analyzed on flow cytometer (Scheme 2).

2.11. Determination of metal ion concentrations

Total concentrations of Al, Fe, Ni, Cr and Cu in the growth medium HAM, electroporation and 2 h incubation media obtained after electroporation of CHO cells with all three pulse protocols were determined by inductively coupled plasma mass spectrometry (ICP-MS) against an external calibration curve as described previously [14] (Scheme 2). Samples were digested with 0.1 ml of 30 % H_2O_2 and 0.1 ml of 65 % HNO_3 (both suprapur, obtained from Merck, Germany), which were added to preweighed plastic tubes containing 0.2 ml of sample. The tubes were then sealed with caps and left overnight at 80 °C. Following digestion, 1.8 ml of Milli-Q water (Direct-Q 5 Ultrapure water system; Merck Millipore, USA) was added, and the tubes were weighed again. Concentration of Al, Fe, Ni, Cr and Cu was determined on Agilent 7900 ICP-MS instruments (Agilent Technologies, Japan). Calibration standard solutions of Al, Fe, Ni, Cr and Cu were prepared from multi-element

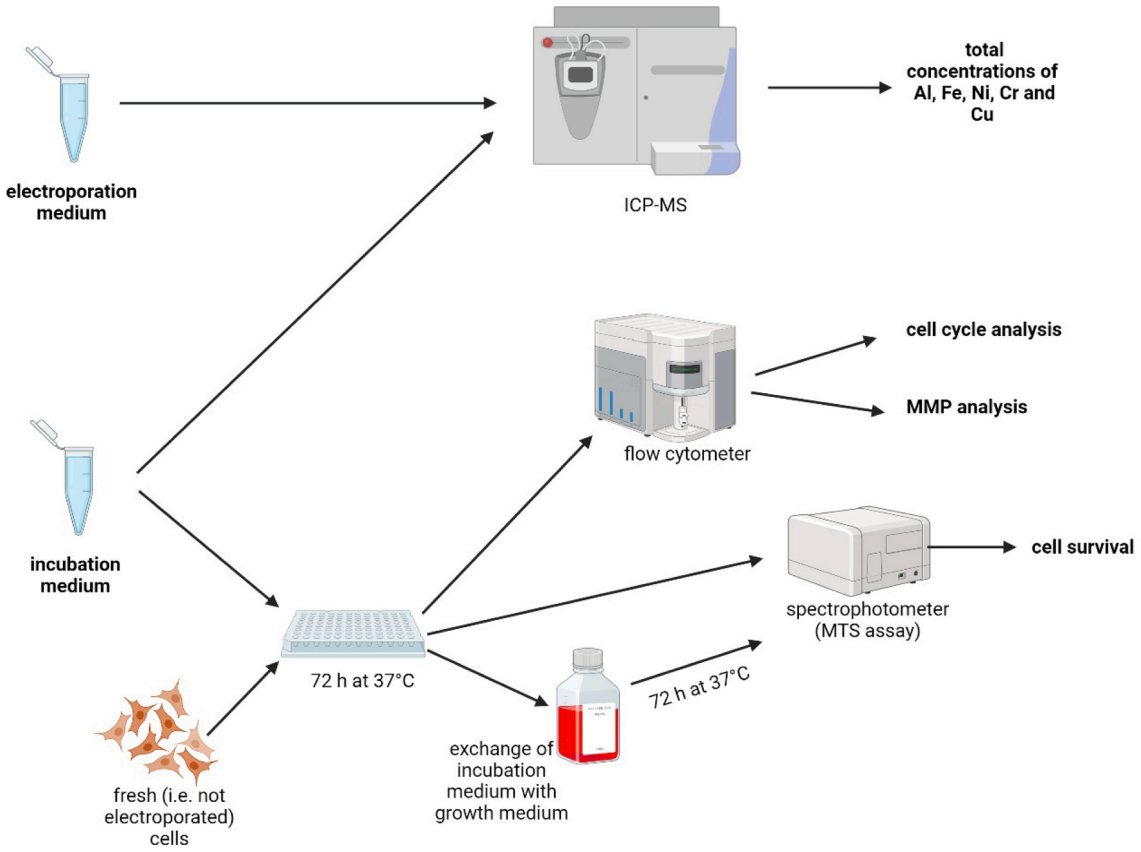

Scheme 2. Schematic overview of assays performed. The total concentrations of aluminum (Al), iron (Fe), nickel (Ni), chromium (Cr), and copper (Cu) in the electroporation and 2-hour incubation media collected after electroporation of CHO cells with each of the three pulse protocols were quantified using inductively coupled plasma mass spectrometry (ICP-MS). Cell cycle analysis and mitochondrial membrane potential (MMP) detection were performed on CHO cells grown in SS, 8 × 5 ms, 2 h incubation medium for 72 h, using a flow cytometer. Survival of CHO and HCT116 cells grown in incubation media obtained after electroporation of CHO or HCT116 cells with all three pulse protocols and both type of electrodes was determined by MTS assay. Additionally, an MTS assay was used to evaluate the survival of CHO cells grown in SS, 8 × 5 ms, 2 h incubation medium for 72 h and then in growth medium for another 72 h. Created in https://BioRender.com.

stock solution (containing 1000 μg/ml of each element in 6.5 % HNO_3). Stock solution was obtained from Merck (Germany). Calibration standards were prepared in 3.25 % HNO_3 (same concentration as in samples).

2.12. Statistical analysis

All results are presented as the mean value from 3 to 5 independent experiments, with data variability expressed as the standard deviation. Statistical analysis was performed using SigmaPlot 11.0 (Systat Software Inc., Chicago, IL, USA). A two-way ANOVA test was employed to compare the experimental groups, with statistical significance set at $p < 0.05$.

3. Results

3.1. Membrane permeabilization and viability of the cells after electroporation

Electroporation with 8 × 5 ms pulse protocol resulted in cell membrane permeabilization and a decrease in viability of CHO cells (Fig. 1, upper) at the lowest electric field compared to other pulse protocols. The HV-BP and the 8 × 100 μs pulse protocol yielded similar permeabilization results and cell viability.

For HCT116 cells (Fig. 1, lower), electroporation with 8 × 5 ms pulse protocol also resulted in cell membrane permeabilization and a decrease in cell viability at the lowest electric field compared to other pulse protocols.

3.2. The viability of non-electroporated cells in incubation medium

Incubation of electroporated cells (different combination of pulse parameters and electrodes) lasted either 2 or 4 h then non-electroporated cells were seeded in the incubation medium for 72 h. Cell viability in incubation medium was determined for both cell lines.

Overall, the viability of non-electroporated CHO cells seeded in the incubation medium obtained by incubating CHO cells electroporated with Al electrodes for 2 or 4 h was never below 70 % (Fig. 2).

Overall, the viability of non-electroporated CHO cells, seeded in the incubation medium obtained after 2 and 4 h of incubation of CHO cells electroporated with SS electrodes was lower than that of cells seeded in the incubation medium obtained with Al electrodes, and was as low as 0 % (Fig. 2). The viability of non-electroporated CHO cells seeded in incubation medium SS, 8 × 100 μs, 2 h, dropped below 60 % at an electric field of 2 kV/cm, while it was above 95 % in incubation medium SS, 8 × 100 μs, 4 h at all tested electric fields (Fig. 2). The viability of non-electroporated CHO cells seeded in incubation medium SS, HV-BP, 2 h and SS, HV-BP, 4 h did not drop below 80 %. However, the exception was viability of the cells at an electric field of 1.75 kV/cm, which dropped below 60 % for both incubation periods. The viability of non-electroporated CHO cells seeded in the incubation medium SS, 8 × 5 ms, 2 h, dropped to 65 % already at an electric field of 0.25 kV/cm. At an electric field of 0.375 kV/cm, even lower cell viability (below 20 %) was measured. At higher electric fields (0.5, 0.625 and 0.75 kV/cm), cell viability was no longer detected. Same trend was detected for cell viability in incubation medium SS, 8 × 5 ms, 4 h.

Overall, the viability of non-electroporated HCT116 cells seeded in

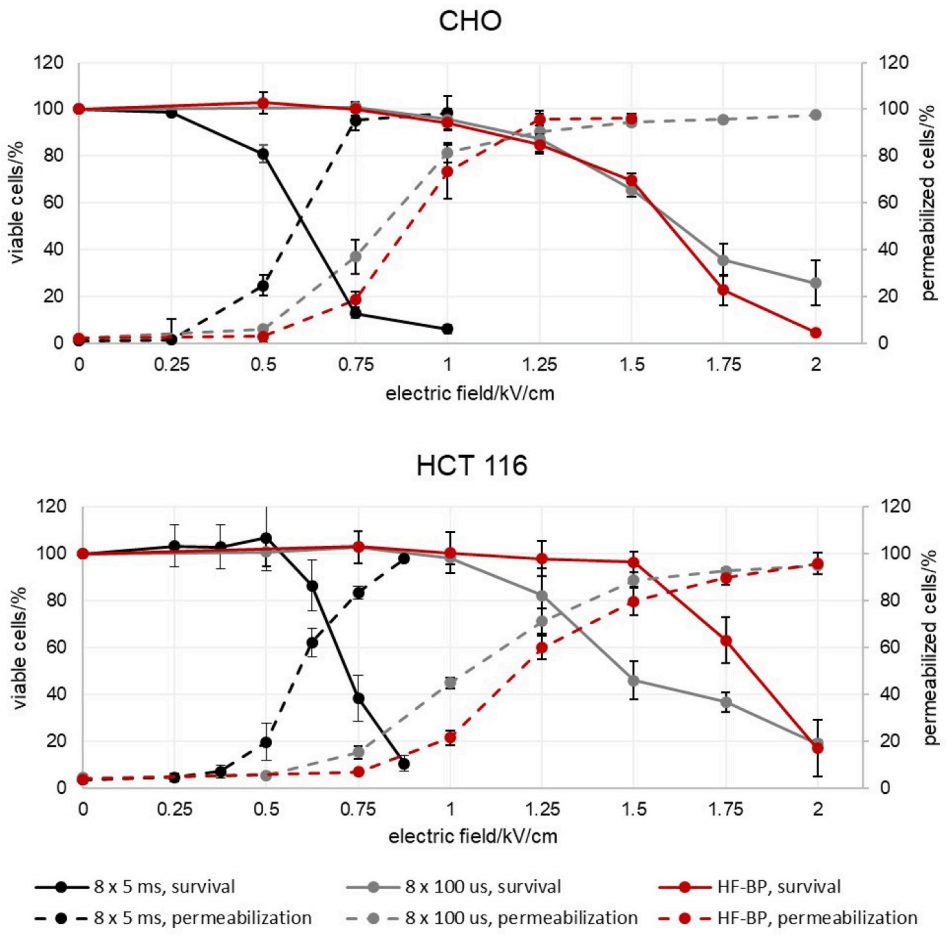

Fig. 1. Permeabilization (dashed lines) and survival curves (solid lines) for CHO (upper) and HCT116 cell line (lower) for all three pulse protocols; 8 × 5 ms (black), 8 × 100 μs (grey) and HV-BP (red). Symbols represent mean and bars standard deviation.

the incubation medium obtained by incubating HCT116 cells electroporated with Al electrodes for 2 or 4 h was never less than 72 % (Fig. 3). The viability of non-electroporated HCT116 cells seeded in the incubation medium Al, 8 × 100 μs, 2 h and Al, 8 × 100 μs, 4 h was mostly above 90 %, with the only exception at an electric field of 1.75 kV/cm and 4 h incubation, where lower cell viability was measured. The viability of non-electroporated HCT116 cells seeded in the incubation media Al, 8 × 5 ms, 2 h, Al, 8 × 5 ms, 4 h, Al, HV-BP, 2 h and Al, HV-BP, 4 h was above 85 % at all tested electric fields.

As in the case of CHO cells, overall, the viability of non-electroporated HCT116 cells seeded in the incubation medium obtained after 2 or 4 h of incubation of HCT116 cells electroporated with SS electrodes was lower compared to cells seeded in the incubation medium obtained with Al electrodes, and was as low as 0 % (Fig. 3). The viability of non-electroporated HCT116 cells seeded in the incubation medium SS, 8 × 100 μs, 2 h and SS, 8 × 100 μs, 4 h dropped below 85 % at electric fields above 1.25 kV/cm and 1.5 kV/cm, respectively. The viability of non-electroporated HCT116 cells seeded in the incubation medium SS, HV-BP, 2 h decreased uniformly with increase of electric field at electric fields above 1.25 kV/cm. The incubation medium SS, HV-BP, 4 h resulted in a similar trend in cell viability with increasing electric field, but the measured cell viability was a few percent higher at all electric field values. The viability of non-electroporated HCT116 cells seeded in incubation medium SS, 8 × 5 ms, 2 h dropped to 60 % at an electric field of 0.5 kV/cm. At an electric field of 0.625 kV/cm even lower cell viability was measured (below 25 %). At a higher electric field (0.75 kV/cm), no cell viability was detected. Same trend was observed for cell viability in incubation medium SS, 8 × 5 ms, 4 h.

Since the incubation medium had a greater effect on the viability of the CHO cell line compared to the HCT166 cell line, experiments in which the incubation medium was replaced with growth medium after 72 h of growth, as well as observations of changes in mitochondrial membrane potential and cell cycle analysis, were performed only on the CHO cell line.

3.3. *Replacement of incubation medium with growth medium, mitochondrial membrane potential and cell cycle*

Replacing the incubation medium (SS, 8 × 5 ms, 2 h) with growth medium after 72 h led to the regrowth of a few cells in the culture (Fig. 4, left). After a further 72 h of growth, an increased cell viability was measured at the electric field of 0.375 kV/cm and 0.5 kV/cm. However, no cell viability was still observed at electric fields of 0.625 and 0.75 kV/cm (using MTS assay and we also did not observe any colonies by visual inspection).

The changes in MMP were examined in CHO cells grown for 72 h in an incubation medium SS, 8 × 5 ms, 2 h obtained at different electric fields (Fig. 4, right). Compared to CHO cells grown in incubation medium obtained at electric field of 0 kV/cm for 72 h, statistically significantly higher median value of the MMP fluorescence was observed in cells incubated in medium obtained at electric field of 0.375 and 0.5 kV/cm. Median value of the MMP fluorescence in cells incubated in medium obtained at electric field of 0.625 and 0.75 kV/cm was lower than in control samples. The addition of CCCP to the experimental samples lead to statistically significantly lower MMP fluorescence. CCCP control resulted in values between 10 and 30 % of the median value of the MMP

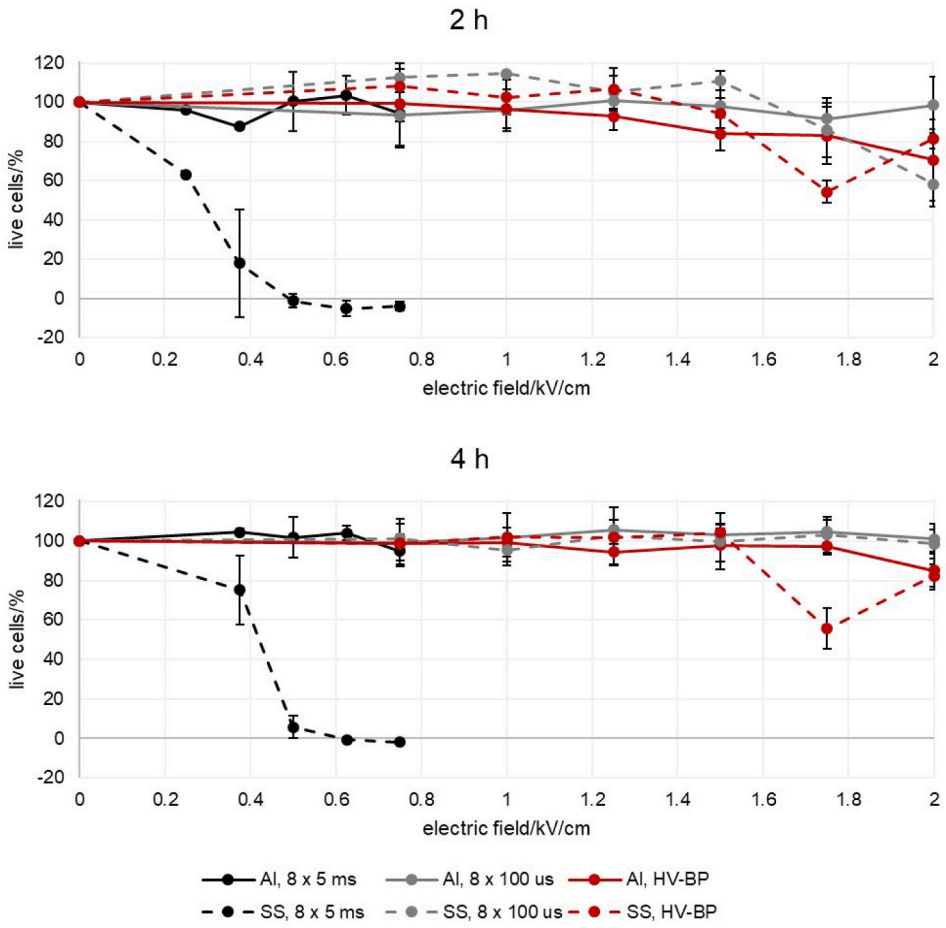

Fig. 2. Percentage of viable non-electroporated cells after 72 h of growth in the incubation medium compared to the control. Non-electroporated CHO cells were seeded in incubation medium obtained by incubating electroporated CHO cells in growth medium for 2 (upper) or 4 h (lower). Three pulse protocols were used for electroporation, 8 × 5 ms (black), 8 × 100 μs (grey) and HV-BP (red), and two electrode materials, SS (dashed lines) and Al (solid lines). For control, non-electroporated CHO cells were seeded in incubation medium obtained by incubating non-electroporated CHO cells in growth medium for 2 or 4 h. The symbols represent the mean and the bars the standard deviation.

fluorescence of control samples, indicating that also samples at 0.625 kV/cm and 0.75 kV/cm still had some viable cells present.

Cell cycle analysis (Fig. 5) was performed after 72 h of CHO cells growth in the incubation media SS, 8 × 5 ms, 2 h. In the incubation medium prepared at an electric field of 0.5 kV/cm, we observed a reduced proportion of cells in the G0/G1 phase and a higher number of events in the sub-G1 phase. For cells grown in incubation media obtained at electric fields of 0.625 kV/cm and higher, there was a noticeable decrease in the S and G2/M phases and a corresponding increase in sub-G1 events. The sub-G1 events represent cells undergoing internucleosomal DNA fragmentation, a hallmark of apoptosis [39]. These results suggest that at electric fields of 0.625 kV/cm and higher, cells are either arrested in the G0/G1 phase or initiated apoptotic pathways.

3.4. The concentrations of metal ions

The concentrations of Fe, Cr, Ni, Al and Cu ions were determined by ICP-MS in the electroporation medium and in the incubation medium (2 h) obtained during/after electroporation of CHO cells with SS electrodes and all three pulse protocols at different electric fields (Scheme 2). The concentrations of Al ions in all analyzed media were below limit of quantification of the applied ICP-MS analytical method, so we do not report their values. The concentrations of Fe, Cr, Ni and Cu in the electroporation media were higher than in incubation media for all pulse protocols. The highest concentrations of all metal ions in both the electroporation and incubation media, were obtained with the 8 × 5 ms pulse protocol (Figs. 6 and 7).

The concentrations of Cr and Cu ions in the electroporation media (Fig. 6) did not significantly increase by the applied electric field in the 8 × 100 μs and HV-BP pulse protocols (Fig. 8, left). Concentrations of approximately 330 ng/ml Cr ions and approximately 30 ng/ml Cu ions were measured at electric fields of 1.5, 1.75 and 2 kV/cm for 8 × 100 μs and HV-BP pulse protocols. For the 8 × 100 μs pulse protocol, Fe and Ni ion concentrations increased with the electric field, reaching up to 1159 ng/ml for Fe and 404 ng/ml for Ni at an electric field of 2 kV/cm. The concentrations of Fe and Ni ions also increased slightly in the HV-BP pulse protocol; up to 528 ng/ml for Fe and 90 ng/ml for Ni at an electric field of 2 kV/cm. The concentrations of all four ions increased with the electric field in the 8 × 5 ms pulse protocol (Fig. 8, right). The concentration of Cr ions increased up to 26.138 μg/ml at an electric field of 0.625 kV/cm. The concentrations were higher than the toxic concentration of Cr(VI) and lower than the toxic concentration of Cr(III) ions, which were reported to be 150 ng/ml and 60 μg/ml, respectively [40]. The Fe ions concentration increased up to 72.637 μg/ml at an electric field of 0.625 kV/cm. The concentrations of Fe ions were still below the determined toxic value of 111.6 μg/ml [19]. The concentration of Ni ions increased to 14.562 μg/ml. The concentrations of Ni ions were above the toxic concentration of 2 μg/ml reported from the scientific literature [41,42]. The concentration of Cu ions increased up to 1.049 μg/ml, which is much lower than the reported toxic value of 10.85 μg/ml [43].

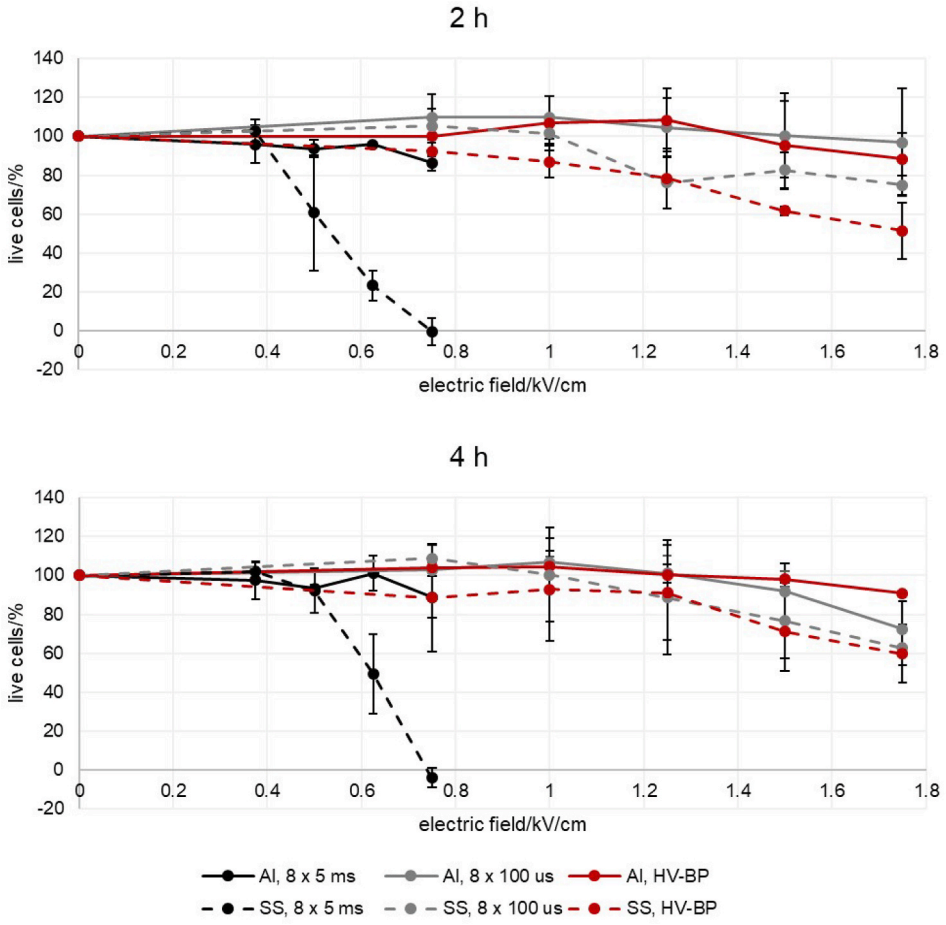

Fig. 3. Percentage of viable non-electroporated cells after 72 h of growth in the incubation medium compared to the control. Non-electroporated HCT116 cells were seeded in incubation medium obtained by incubating electroporated HCT116 cells in growth medium for 2 (upper) or 4 h (lower). Three pulse protocols were used for electroporation, 8 × 5 ms (black), 8 × 100 μs (grey) and HV-BP (red), and two electrode materials, SS (dashed lines) and Al (solid lines). For control, non-electroporated HCT116 cells were seeded in incubation medium obtained by incubating non-electroporated HCT116 cells in growth medium for 2 or 4 h. The symbols represent the mean and the bars the standard deviation.

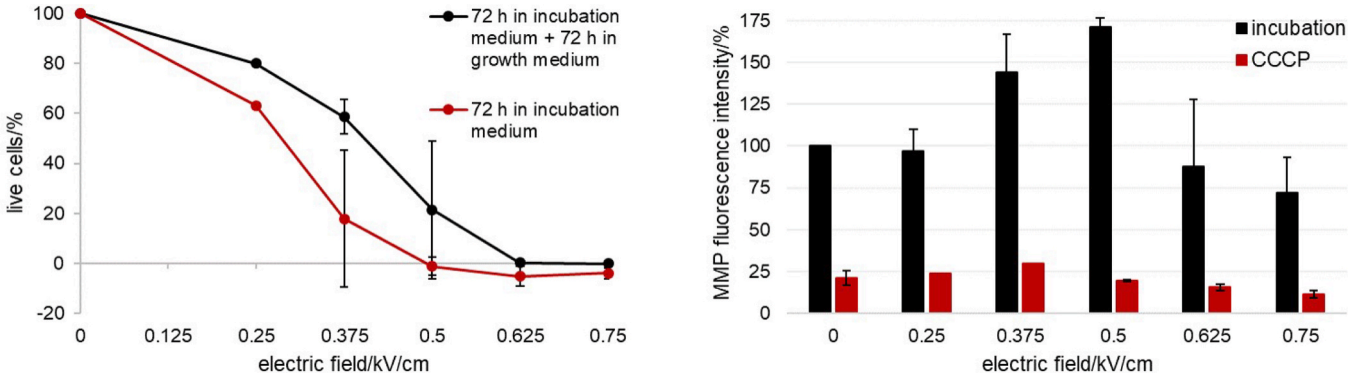

Fig. 4. Left: Proportion of viable cells compared to control. Non-electroporated CHO cells were seeded in SS, 8 × 5 ms, 2 h incubation medium. The cells were grown in the incubation medium for 72 h (red curve). After 72 h of growth, the incubation medium was replaced by growth medium. The viability of the cells was determined after further 72 h (black curve). Symbols represent the mean and bars the standard deviation. Right: Changes in MMP in CHO cells (black) grown for 72 h in SS, 8 × 5 ms, 2 h incubation medium obtained at different electric fields. The median value of the MMP fluorescence intensity of the samples is normalized to the median value of the MMP fluorescence intensity of the control samples (cells, grown in incubation medium obtained at electric field of 0 kV/cm). CCCP-positive controls are presented in red. The mean values of three experiments are shown with the corresponding standard deviations (bars).

The concentrations of metal ions in the incubation media (Fig. 7) did not significantly increase by the applied electric field in the 8 × 100 μs pulse protocols. Concentrations of about 5 ng/ml Cr ions, 246 ng/ml Fe ions, 5 ng/ml Ni ions (Fig. 9, left) and 12 ng/ml Cu ions were determined. In the HV-BP pulse protocol, the concentrations of Fe, Cu, Ni and Cr ions were about 190 ng/ml, 11 ng/ml, 2 ng/ml and 5 ng/ml respectively. Only at an electric field of 1.75 kV/cm slightly higher concentrations were determined. At 8 × 100 μs and HV-BP pulse

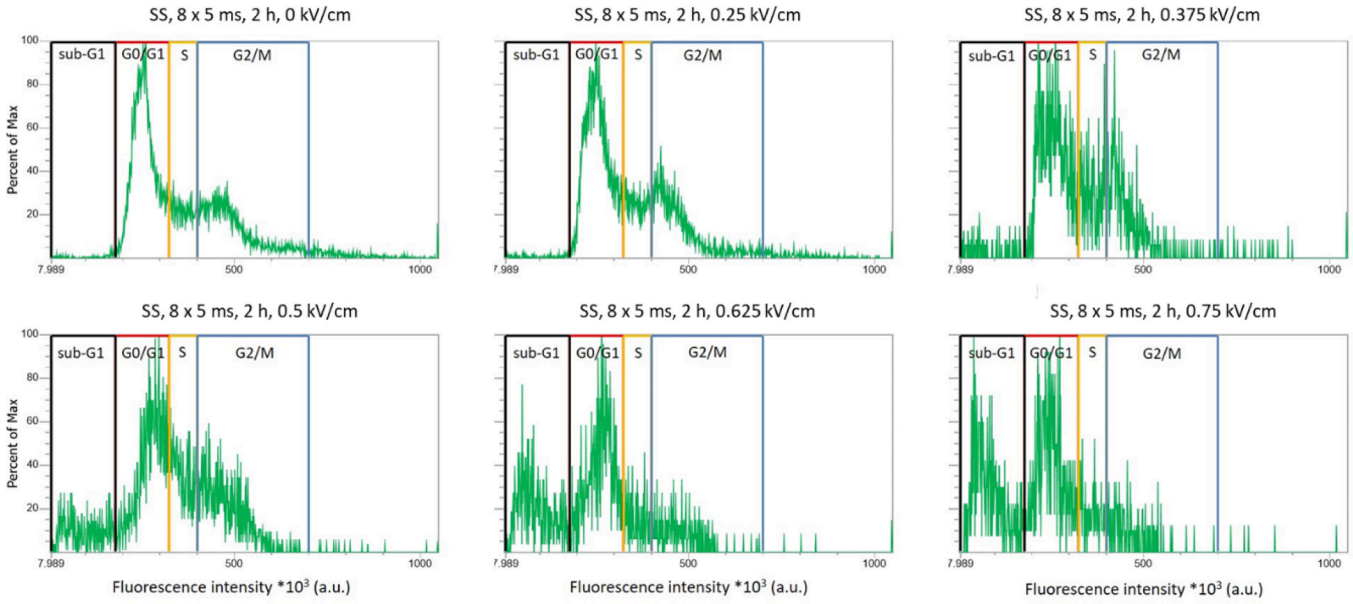

Fig. 5. The proportion of CHO cells in different cell cycle phases. CHO cells were grown for 72 h in incubation medium SS, 8 × 5 ms, 2 h obtained at different electric fields.

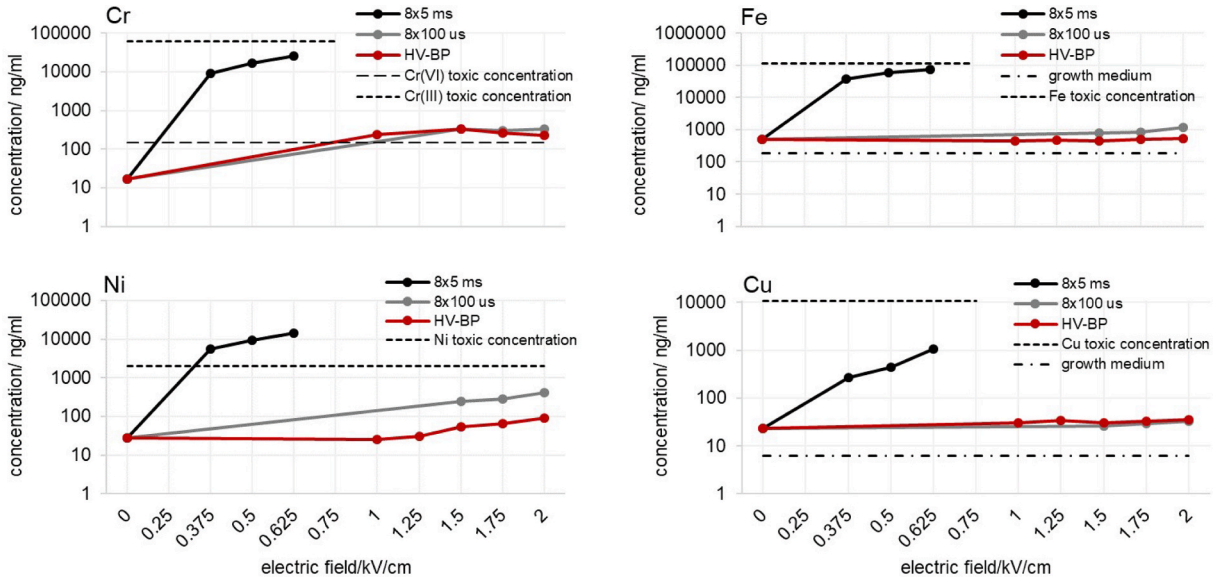

Fig. 6. The concentrations of metal ions in the electroporation medium collected after electroporation of CHO cells suspension using SS electrodes and three pulse protocols: 8 × 5 ms, 8 × 100 μs and HV-BP. The dashed (and long dashed) line indicates the toxic concentration of the ion reported from the scientific literature [19,40,41,42,43]. The dash-dotted line indicates the ion concentration in the growth medium. The concentration of Cr ions and the concentration of Ni ions in the growth medium were below the limit of quantification of ICP-MS.

protocols, the concentrations of metal ions in the incubation media did not exceed toxic levels (Fig. 7). The concentrations of all four ions increased with the electric field in the 8 × 5 ms pulse protocol. The concentration of Cr ions increased up to 3031 ng/ml at an electric field of 0.75 kV/cm (Fig. 9, right). The concentrations were higher than the toxic concentration of Cr(VI) ions (150 ng/ml) at electric fields of 0.375 kV/cm and above and lower than the toxic concentration of Cr(III) ions (60 μg/ml). The concentrations of Fe, Ni and Cu ions increased to 1.068 μg/ml, 1.179 μg/ml and 102 ng/ml respectively (Fig. 9, right). At all electric fields the concentrations of Fe, Ni and Cu ions were lower than the toxic values specified for these ions (Fig. 7).

4. Discussion

In our study, we focused on the effects of post-electroporation metal (by)products that are formed during cell recovery or activation of cell death pathways within 2 to 4 h after electroporation and are subsequently released into the surrounding (incubation) medium. These post-electroporation metal byproducts have the potential to affect otherwise non-electroporated nearby cells, thereby extending the impact of electroporation beyond the initially targeted cells.

We investigated the survival of non-electroporated cells seeded for 72 h in incubation medium obtained from cells electroporated either with Al or with SS electrodes (Scheme 1). The incubation medium obtained from cells electroporated with Al electrodes, regardless of the

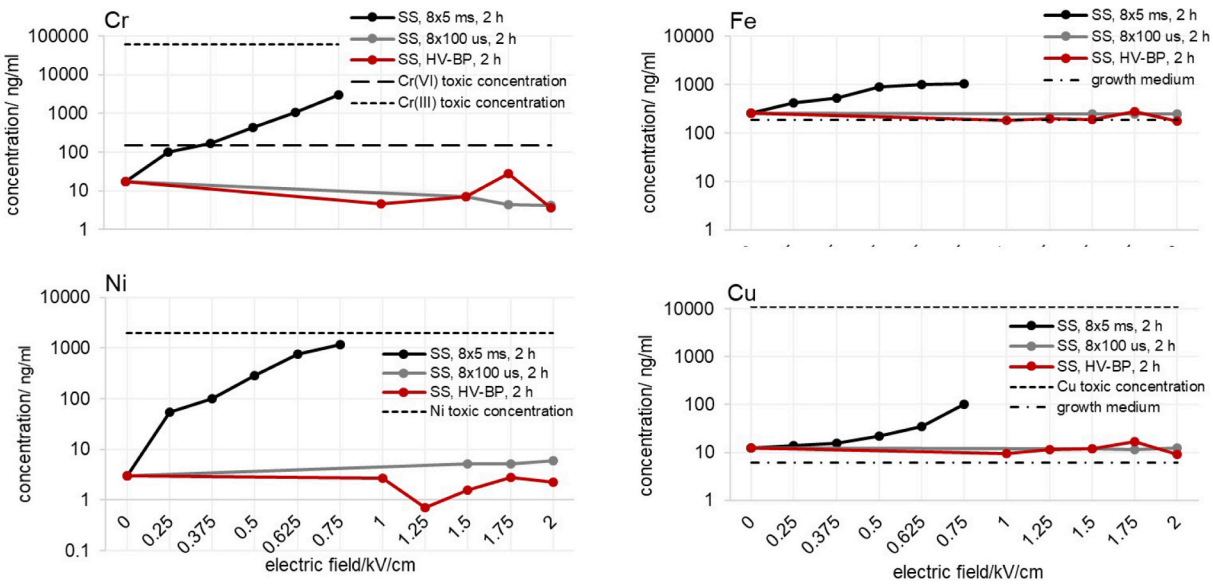

Fig. 7. The concentration of metal ions in SS, 8 × 100 μs, 2 h, SS, 8 × 5 ms, 2 h and SS, HV-BP, 2 h incubation media. The dashed (and long dashed) line shows the toxic concentration of the ion reported from the scientific literature [19,40,41,42,43]. The dash-dotted line shows the ion concentration in the growth medium. The concentration of Cr ions and the concentration of Ni ions in the growth medium were below limit of quantification of ICP-MS.

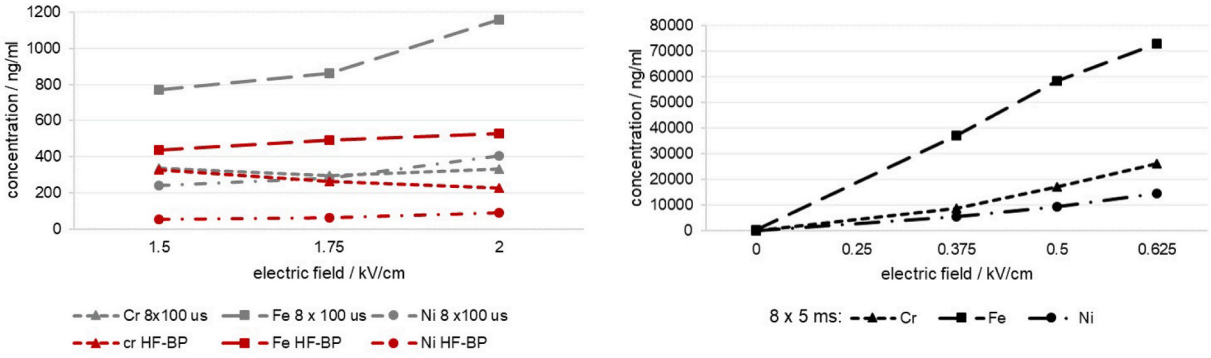

Fig. 8. Left: The concentrations of metal ions (Cr, Fe and Ni) in the electroporation medium collected after electroporation of CHO cells suspension using SS electrodes and pulse protocols 8 × 100 μs and HV-BP. Right: The concentrations of metal ions (Cr, Fe and Ni) in the electroporation medium collected after electroporation of CHO cells suspension using SS electrodes and pulse protocols 8 × 5 ms.

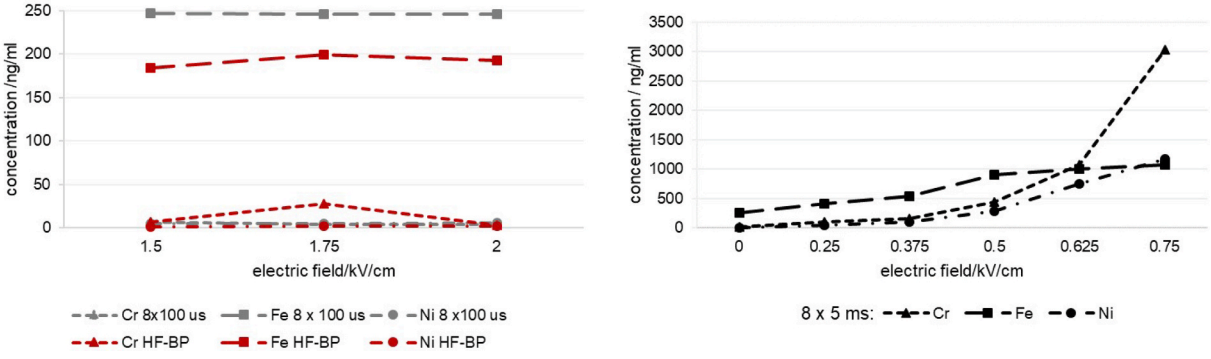

Fig. 9. Left: The concentrations of metal ions (Cr, Fe and Ni) in SS, 8 × 100 μs, 2 h and SS, HV-BP, 2 h incubation media. Right: The concentration of metal ions (Cr, Fe and Ni) in SS, 8 × 5 ms, 2 h incubation medium.

electric pulse protocol, electric field strength, or cell line, showed minimal to no effect on the cell growth. In contrast, the incubation medium collected from cells electroporated with SS electrodes influenced cell growth, with the extent of this effect depending on the specific electric pulse protocol, the electric field applied during electroporation, and the cell line used (Figs. 2 and 3). Since the influence of the incubation medium on cell growth depended on the electrodes used, we linked it to the metal ions released during electric pulse delivery and excreted out of and from electroporated cells during the incubation. We measured the amount of metal ions only in 2-hour incubation media, because they had

slightly larger effect on metabolic activity of the cells than 4-hour incubation media. Measurements of amount of metal ions (Fe, Cr, Ni, Al, Cu) in incubation media obtained after 2-hour incubation of CHO cells electroporated with SS electrodes confirmed, that amounts of all metal ions were considerably higher in incubation media in comparison to growth medium. The increase in metal ion concentration in incubation media depended on the electric pulse protocol and the electric field strength during cell exposure to electric pulses.

4.1. Metal ions in electroporation media

The extent of chemical changes in electroporation medium depends on the protocol of electric pulses, which has been focus of most of previous studies [14,32,44]. The studies also addressed the consequences of lipid oxidation and production of ROS as well as the electrochemical reactions that take place on the electrodes during the application of electric pulses and the effects of the resulting products on the success of the desired electroporation application [15,21,24,28,44,45,46,47]. It has been shown previously that, with the same electroporation parameters, the amount of Al ions released from Al electrodes during the delivery of electric pulses is less toxic than the amount of Fe ions released from SS electrodes [13,19]. Moreover, Saulis et al [19] have shown that growth medium treated with electric pulses using Al electrodes is considerably less toxic than when treated with SS electrodes. Our results are in line with their observations.

Previous studies [14,15,19,32] have also shown a significant increase in the concentrations of metal ions in electroporation media when SS electrodes are used, whether in the presence of medium alone or with cells exposed to electric pulses. Cell viability in such electroporation media has been reported to decrease inversely with the amount of electric charge passing through the solution [19]. This decline in viability has been primarily attributed to the high concentrations of Fe ions released during pulse delivery [15,19]. However, cell viability remains significantly higher in media supplemented with the same concentration of Fe(III) ions as those found in toxic levels after electroporation with SS electrodes. This suggested that other factors might also contribute to the cytotoxicity of the electroporation medium [19].

Our findings indicated that when SS electrodes were used, the concentration of Fe ions in the electroporation medium did not exceed toxic level for any of the applied pulse protocols (Fig. 6). The amount of Fe ions released during the 8 × 5 ms pulse protocol approached toxic level. A pulse protocol with similar electroporation efficiency, consisting of the same number of pulses that are 50 times shorter (8 × 100 μs) and delivered at the same repetition rate, resulted in the release of 100 times fewer Fe ions. When using bipolar pulses (BP-HV), which offer comparable electroporation efficiency, the amount of released Fe ions was reduced even further to half the amount released by the 8 × 100 μs pulse protocol. These findings are consistent with earlier reports that the duration and polarity of electric pulses significantly influence the amount of metal ions released during electroporation [13,14,32].

Although the amount of Cr ions released into the electroporation media during the studied pulse protocols was smaller than the amount of Fe ions, the Cr ion concentrations exceeded the toxic threshold for Cr(VI) ions in all tested protocols but remained below the toxic threshold for Cr (III) ions (Fig. 6). In the case of 8 × 5 ms pulse protocol the ratio of released Fe to Cr ions decreased with increasing electric field strength indicating that Cr ions release is more intensified by the electric field compared to Fe ions (Fig. S1, left). The opposite trend was observed with the 8 × 100 μs and HF-BP pulse protocols, where the Fe/Cr ion ratio in the electroporation medium increased with the electric field but remained lower than the ratio in bulk SS alloy. Similar to Cr ions in 8 × 5 ms pulse protocol the Fe/Ni ion ratio in the electroporation medium decreased with increasing electric field (Fig. S1, left).

4.2. Corrosion at different pulse parameters

The differences in the dynamics of metal ion release during electrode dissolution can be linked to various forms of corrosion that occur during the application of electric pulses of different durations. The corrosion resistance of SS is primarily attributed to the spontaneous formation of a passive film on its surface [48]. Under normal conditions, this passive film is approximately 2 nm thick and consists predominantly of hydrated Cr-rich oxide (Cr_2O_3) or oxyhydroxide (CrO(OH)) species, with smaller amounts of Fe oxides (Fe_2O_3, FeO) and oxyhydroxides (FeO(OH)). Ni oxide (NiO) may also be present, though it is less common than Cr or Fe oxides [49,50]. The formation energy of these metal oxides reflects the metals' affinity for oxygen, providing a quantitative measure of the driving force behind oxidation. Due to Cr oxide's lower formation energy in SS alloys, it tends to dominate in Cr-containing steels [50]. The composition, structure, and thickness of the passive film are influenced not only by the alloy composition but also by environmental factors such as pH, the presence of various ions and proteins, temperature, surface roughness, aging, and repeated usage of the electrodes [51,52,53,54,55]. It is commonly reported that the surface oxide layer of SS exhibits a bilayer structure, with an inner layer rich in trivalent Cr and an outer layer rich in ferric compounds [50]. Beneath this passive film, the alloy surface layer becomes enriched also with Ni.

However, at higher potentials, such as those encountered during the delivery of electroporation pulses or in highly oxidizing environments with high-temperature electrolytes, the passive film can break down, leading to general corrosion due to transpassive dissolution [56]. The protective effect of the passive film is lost when Cr(III) is oxidized to Cr (VI), forming highly soluble CrO_3. When CrO_3 comes into contact with water at neutral to slightly alkaline conditions (pH 7.4), it reacts with water to form H_2CrO_4, which dissociates into CrO_4^{2-} species. The SS surface then becomes covered by a mixed film of oxyanion CrO_4^{2-} and Fe (III) oxide. The oxyanion CrO_4^{2-} is stable and highly mobile in aquatic environments. However, in the presence of electron donors, such as Fe (II) ions, CrO_4^{2-} can be readily reduced to Cr(III) [57], which, under neutral to alkaline pH conditions, forms the insoluble hydroxide Cr $(OH)_3$. The extent of reduction depends on the concentration of Fe(II) ions in the solution, which also influences the equilibrium concentrations of Cr(VI) and Cr(III) species [57]. Similar to Cr(III) species, Fe(III) oxides are also largely insoluble in neutral to alkaline solutions and tend to precipitate as less mobile $Fe(OH)_3$ or Fe oxides, which help maintain the concentration of Fe ions in equilibrium near the alloy surface. Cr(VI) compounds, due to their high solubility and mobility, diffuse away from the electrode surface more readily, increasing the rate of Cr release. The rate of Cr(VI) oxide dissolution exceeds the rate of its formation, causing a drastic increase in anodic current density. Without a stable protective oxide film, SS actively corrodes [50,58,59]. Environmental factors such as pH, temperature, and chloride concentration significantly influence this breakdown process [56]. $Cr_2O_7^{2-}$ and CrO_4^{2-} oxyanions are strong oxidants that are highly reactive with proteins in aqueous solutions. They can oxidize thiol groups, induce protein cross-linking, generate reactive oxygen species (ROS), and bind to various amino acid residues, resulting in protein damage. Additionally, they can oxidize unsaturated lipids. All these effects contribute to the toxic and carcinogenic effects of Cr(VI). Nickel, present in the original electrodes, tends to remain stable as $Ni(OH)_2$ or NiOOH, leading to its retention in the initial electrode while forming surface (hydro)oxides.

Our results suggest that in the 8 × 100 μs and HV-BP pulse protocols, a transpassive film likely forms, as indicated by the lower Fe/Cr ion release ratio compared to bulk SS. This ratio increases with the electric field applied to the electrodes (Fig. 8, left), consistent with published model calculations and experimental data [60]. In contrast, with the 8 × 5 ms pulse protocol, passivity breakdown and general corrosion occur at lower electric fields. At 0.375 kV/cm, the Fe/Cr ion release ratio matches that of the bulk alloy, indicating that toxic Cr(VI) species are already being formed at low electric fields. As the electric field increases,

the Fe/Cr ion release ratio in the electroporation medium decreases (Fig. S1, right), suggesting the formation of increasing amounts of Cr compounds.

4.3. Metal overload of electroporated cells

According to our experimental protocol, additional metal ions and their secondary reaction products, including precipitates rich in Fe, Cr, and Ni ions, were present in the surrounding medium of electroporated cells. During pulse delivery and the subsequent 5-minute recovery period, these ions can easily permeate the electroporated cells, leading to metal overload and disrupting cellular homeostasis. Furthermore, these ions can adsorb onto the cell membrane surface through electrostatic interactions; positively charged ions interact with negatively charged phosphate groups in the lipid bilayer, and negatively charged ions (such as chromate and dichromate) interact with positively charged regions on membrane proteins. These interactions can further destabilize the lipid bilayer, inducing oxidative damage to lipids, interfere with membrane-bound enzymes or transport proteins and other membrane components, ultimately leading to lipid peroxidation. Additionally, Cr (VI) ions can enter cells via anion transporters that normally facilitate the exchange of sulfate (SO_4^{2-}) and phosphate (PO_4^{3-}) ions across the membrane. Due to their similar charge and size, chromate and dichromate ions can be mistakenly transported into the cell by these transporters [61]. Similarly, soluble Ni compounds (Ni(II)) can enter cells through calcium channels [29] while some forms of Ni are endocytised [62].

4.4. Fe, Cr and Ni compounds toxicity and cellular transport

A common factor in the toxicity and carcinogenicity of Fe, Cr, and Ni compounds is their ability to generate ROS and reactive nitrogen species. For Fe and Cr, toxicity is primarily driven by mechanisms such as the Fenton reaction and the production of superoxide and hydroxyl radicals, with significant effects occurring in mitochondria, microsomes, and peroxisomes. Hexavalent Cr (Cr(VI)) reacts with glutathione to form pentavalent (Cr(V)) and tetravalent (Cr(IV)) Cr species in plasma and organelle membranes [63]. Additionally, Cr(VI) reacts with NADH/NADPH within mitochondria, further contributing to the formation of Cr (V). Cr(V) and Cr(IV) species (both directly and indirectly) induce DNA double-strand breaks, activating DNA damage signaling sensors, mitochondrial apoptosis, and the ataxia-telangiectasia-mutated (ATM) and ataxia-telangiectasia-Rad3-related (ATR) pathways. These pathways result in cell cycle arrest primarily in the S-phase and G2/M phase to prevent the replication and segregation of damaged DNA. Cr(IV) may be particularly potent, as it causes DNA breaks and somatic recombination without necessarily inducing apoptosis. If apoptosis and DNA repair mechanisms fail, the damaged cells may become immortalized, leading to loss of heterozygosity and increased genetic plasticity. In contrast, Ni (Ni(II)) toxicity primarily results from glutathione depletion and the binding of Ni to sulfhydryl groups of proteins such as cysteine, which is also a target of Cr(III) [29,64].

Among the ions analyzed in this study (Fe, Cr, Ni, and Cu), Fe has been the most extensively studied regarding cellular transport. A key component of cellular Fe trafficking is the Fe-storage protein ferritin [65]. While specialized cells like hepatocytes or macrophages possess ferroportin, a transmembrane protein that exports Fe from the cell [66], CHO cells, being non-specialized in Fe metabolism, lack such mechanisms. Recent studies [33,34] have indicated that excess Fe can also be secreted via EVs, and the uptake of these EVs can induce oxidative damage in recipient cells. Mitochondria-derived vesicles (MDVs) are potential mediators for loading mitochondrial Fe into EVs, and Fe-loaded ferritin is secreted through both nonclassical secretory autophagy and multivesicular body–exosome pathways [67].

For Cr, previous studies have shown that Cr(VI) undergoes a series of reduction reactions within the cell, eventually being reduced to Cr(III), with Cr(V) and Cr(IV) as intermediates [68]. Cr(III) is bound by low-molecular-weight substances within the cell and is eventually transported out, although the exact transporter is unknown [69,70]. So, it is likely that cells use a combination of sequestration, exocytosis, chelation, and autophagy to manage and remove excess Cr compounds (including $CrPO_4$).

Ni ions (Ni(II)) can bind to the thiol (−SH) group of cysteine in glutathione, forming a stable complex that reduces the metal's reactivity and potential toxicity. This complex can then be bound to specific transporters that use ATP to transport it across the cell membrane. The Ni(II)-cysteine complex is stable, and these complexes can aggregate and precipitate out of solution [71].

4.5. Metal ions in incubation media

Due to the significant metal overload in electroporated cells, an increased concentration of metal ions was also expected in the incubation medium (Figs. 7 and 9). During the incubation period, the cells repaired their damaged membranes and re-established homeostasis, or cell death pathways were activated which included the elimination of metal ions overload. This process may involve shedding of metal ions during membrane repair and their inclusion in apoptotic bodies. In the case of SS, 8 × 5 ms, 2 h the concentration of Fe ions in the incubation medium increased linearly, whereas the concentrations of Cr and Ni ions increased even faster with their respective levels in the electroporation medium (Fig. S1, right). For example, at electric field strength of 0.75 kV/cm, the Cr ion concentration in the incubation medium (3031 ng/ml) was three times higher than that of Fe ions (1068 ng/ml). This suggests that the export of Cr and Ni compounds from the cells during the 2-hour post-electroporation recovery period was more intensive than the export of Fe compounds.

Our results indicated that the impact of the incubation medium, obtained from cells electroporated with SS electrodes, on cell growth varied depending on the electric pulse protocol, field strength used for electroporation, incubation time of the electroporated cells, and the cell line. Incubation media from cells electroporated with 8 × 100 μs pulse protocol generally showed no significant effect on cell growth, only a slight reduction in cell viability was observed at higher electric field strengths (Figs. 2 and 3). Interestingly, the incubation medium obtained after 4 h of incubation had a slightly smaller effect on cell growth compared to the 2 h of incubation. It seems that the incubation medium SS, 8 × 5 ms, 2 h and SS, 8 × 5 ms, 4 h impaired the growth of CHO cells to a greater extent compared to HCT116 cells.

4.6. SS, 8 × 5 ms, 2 h incubation medium affect cell viability, cell cycle and MMP

Since the experiments on the influence of the incubation medium on cell growth were assessed using the MTS assay which detects metabolically active cells, the low number of viable cells may be due to reduced cell division or cell cycle arrest that resulted in reduced metabolic activity of the overall sample. When the incubation medium where cells had grown for 72 h was replaced with fresh growth medium, and the cells were grown for an additional 72 h (Fig. 4, left), some cells (previously exposed to incubation media prepared at electric fields of 0.375 kV/cm and 0.5 kV/cm), divided again, as evidenced by the formation of small colonies. This regrowth of cells in their normal conditions confirmed that some cells induced cell cycle arrest in the incubation medium. However, cells that had been incubated in the incubation media prepared at electric fields of 0.625 kV/cm and 0.75 kV/cm did not resume cell division, even after the incubation medium was replaced with fresh growth medium. Cell cycle analysis (Fig. 5) revealed that cell populations exposed to incubation media prepared with electric fields of 0.5 kV/cm and above showed an increasing number of events in the sub-G1 phase as the electric field strength increased. Sub-G1 events indicate internucleosomal DNA fragmentation, a key marker of apoptosis [39].

Our findings suggested that at electric fields of 0.625 kV/cm and higher, cells either became arrested in the G0/G1 phase or initiated apoptotic pathways. Terpilowska and Siwicki [72] reported similar findings in cell cultures treated with 200 μM of chromium chloride and 1000 μM of iron chloride, where an increase in sub-G1 and G0/G1 phase was observed, along with a decrease of MMP. Both effects were attributed to ROS generation. Fe(III) induces the formation of lipid hydroxyl-peroxides and lipid peroxidative products, which generate long-lived lipid radicals that contribute to chronic cell toxicity by attacking biomolecules and organelles, including membrane phospholipids, DNA, and mitochondria. While Fe(III) interacts with DNA bases, Cr(III) binds to both DNA bases and phosphate groups, leading to potentially synergistic damage. Despite the incubation media produced at 0.625 kV/cm and 0.75 kV/cm having similar Cr ion concentrations and significantly lower Fe ion concentrations, our findings align with the reported effects. It's also important to note that the incubation medium contained substantial amounts of Ni ions, which are known to cause G2/M cell cycle arrest and a dose-dependent reduction in MMP [73]. The presence of Ni compounds could contribute either synergistically or antagonistically to the overall cellular effects observed in our study.

G0/G1 −phase cell-cycle arrest results in a transient decrease of DNA synthesis [74] and can be a consequence of ATP production reduction. Namely, Marcussen and colleagues reported on ATP concentration oscillation along the progression of the cell cycle, reaching a peak at G_2/M- and minimum at late G1/early S-phase [75]. Late G1/early S-phase is also accompanied by elevated cytoplasmic pH (up to 7.4) [76].

In cells grown for 72 h in incubation media SS, 8 × 5 ms, 2 h (0.375 kV/cm and 0.5 kV/cm) also statistically significant increase in the MMP was observed (Fig. 4, right). Mitochondrial hyperpolarization can occur for several reasons. Khaled et al. [77] reported that intracellular alkalinization induces hyperpolarization and total cellular ATP loss, as ATPase shifts to reverse proton pumping, using ATP hydrolysis to expel protons from the mitochondrial matrix. Depending on membrane polarization and ADP/ATP levels, ATPase can either synthesize or consume ATP [78]. Phosphate starvation [79], cysteine deprivation leading to lipid peroxide accumulation and ferroptosis [71], and Fe overload-induced mitochondrial damage [80] are other triggers of hyperpolarization. Due to Ni(II) and Cr(III) binding to cysteine, and possibility for insoluble $CrPO_4$ formation, cysteine or phosphate deprivation might be the reason(s) for increased MMP. Mitochondrial hyperpolarization represents significant metabolic stress and is often the earliest change associated with apoptosis pathways [77,81]. It also contributes to the generation of ROS, which can increase susceptibility to apoptosis [82,83]. The mechanisms causing the MMP change in cells exposed to the incubation medium are likely to be different from the mechanisms causing the MMP change in electroporated cells. Namely, we recently reported that MMP is decreased in reversibly and irreversibly electroporated cells [84].

5. Conclusions

During electroporation with SS electrodes and milliseconds pulses high concentrations of Fe, Cr, and Ni ions are released from the electrodes. Consequently, electroporated cells experience metal overload. During the repair of cell membrane or initiation of cell death pathways, if recovery fails, these cells release metal byproducts into their surroundings. The released metal byproducts impact neighboring untreated cells (i.e. cells that were not electroporated), inducing cell death or cell cycle arrest. The toxicity arises from the combined effects of metal ions on cellular functions and the mechanisms that cells use to protect themselves against metal overload.

Although our study was conducted under *in vitro* conditions, it is important to note that metal byproducts can also form under *in vivo* conditions. In ablation procedures that utilize long millisecond electric pulses, such metal byproducts may contribute to cell death and the enlargement of the ablated area. However, special attention should be given to the potential undesired toxic effects of certain metal chemical compounds.

CRediT authorship contribution statement

Alenka Maček Lebar: Writing – review & editing, Writing – original draft, Visualization, Validation, Methodology, Investigation, Formal analysis, Data curation, Conceptualization. **Tjaša Potočnik:** Writing – review & editing, Investigation. **Janez Ščančar:** Writing – review & editing, Investigation. **Stefan Marković:** Writing – review & editing, Investigation. **Tamara Polajžer:** Writing – review & editing, Investigation.

Funding

This research was supported by Slovenian Research Agency (ARRS); research core funding No. P2-0249. Experiments were performed within Infrastructure Program: Network of research infrastructure centers at University of Ljubljana [MRIC UL IP-0510].

Declaration of competing interest

The authors declare that they have no known competing financial interests or personal relationships that could have appeared to influence the work reported in this paper.

Acknowledgements

Authors would like to thank T. Turk and D. Hodžić for their help in the cell culture laboratory.

Appendix A. Supplementary data

Supplementary data to this article can be found online at https://doi.org/10.1016/j.bioelechem.2025.108940.

Data availability

Data will be made available on request.

References

[1] T. Kotnik, L. Rems, M. Tarek, et al., Membrane electroporation and electropermeabilization: Mechanisms and models, Annu Rev Biophys 48 (2019) 63–91.
[2] E. Neumann, M. Schaefer-Ridder, Y. Wang, P.H. Hofschneider, Gene transfer into mouse lyoma cells by electroporation in high electric fields, EMBO J. 1 (1982) 841–845.
[3] Miklavčič D, Mali B, Kos B, et al. Electrochemotherapy: from the drawing board into medical practice. Biomed Eng OnLine 2014; 13(1):29; doi: 10.1186/1475-925X-13-29.
[4] R.V. Davalos, I.L.M. Mir, B. Rubinsky, Tissue ablation with irreversible electroporation, Ann Biomed Eng 33 (2) (2005) 223–231, https://doi.org/10.1007/s10439-005-8981-8.
[5] Geboers B, Scheffer HJ, Graybill PM, et al. High-voltage electrical pulses in oncology: Irreversible electroporation, electrochemotherapy, gene electrotransfer, electrofusion, and electroimmunotherapy. Radiology 2020;295(2):254–272; doi: 10.1148/radiol.2020192190.
[6] K.R.J. Chun, D. Miklavčič, K. Vlachos, et al., State-of-the-art pulsed field ablation for cardiac arrhythmias: ongoing evolution and future perspective, Europace 26(6): euae134 (2024).
[7] C. Rosazza, S. Haberl Meglic, A. Zumbusch, et al., Gene electrotransfer: A mechanistic perspective, Curr Gene Ther 16 (2) (2016) 98–129, https://doi.org/10.2174/1566523216666160331130040.
[8] Kotnik T, Frey W, Sack M, et al. Electroporation-based applications in biotechnology. Trends Biotechnol 2015; 33(8):480–488; doi: 10.1016/j.tibtech.2015.06.002.
[9] S. Mahnič-Kalamiza, E. Vorobiev, D. Miklavcic, Electroporation in food processing and biorefinery, J Membr Biol 247 (2014), https://doi.org/10.1007/s00232-014-9737-x.
[10] Rubinsky L, Guenther E, Mikus P, et al. Electrolytic effects during tissue ablation by electroporation. Technol Cancer Res Treat 2016; 15(5):NP95–NP103.

[11] Lv Y, Zhang Y, Rubinsky B. Molecular and histological study on the effects of electrolytic electroporation on the liver. Bioelectrochemistry 2019; 125:79–89.
[12] K. Balantič, P. Kramar, D. Miklavčič, In silico numerical model of aluminum and iron dissolution during electric pulse application for electroporation, Bioelectricity 6 (1) (2024), https://doi.org/10.1089/bioe.2023.0026.
[13] T. Kotnik, D. Miklavcic, L.M. Mir, Cell membrane electropermeabilization by symmetrical bipolar rectangular pulses. Part II. Reduced Electrolytic Contamination, Bioelectrochemistry 54 (1) (2001) 91–95, https://doi.org/10.1016/s1567-5394(01)00115-3. PMID: 11506979.
[14] A. Vižintin, J. Vidmar, J. Ščančar, D. Miklavčič, Effect of interphase and interpulse delay in high-frequency irreversible electroporation pulses on cell survival, membrane permeabilization and electrode material release, Bioelectrochemistry 134 (2020) 107523, https://doi.org/10.1016/j.bioelechem.2020.107523.
[15] R. Rodaitė-Riševičienė, R. Saulė, V. Snitka, G. Saulis, Release of iron ions from the stainless steel anode occurring during high-voltage pulses and its consequences for cell electroporation technology, IEEE Trans. Plasma Sci. 42 (1) (2014) 249–254, https://doi.org/10.1109/TPS.2013.2287499.
[16] Phillips M, Rubinsky L, Meir A, et al. Combining electrolysis and electroporation for tissue ablation. Technol Cancer Res Treat 2015; 14(4):395–410; doi: 10.1177/1533034614560102.
[17] N.R. Perkons, E.J. Stein, C. Nwaezeapu, et al., Electrolytic ablation enables cancer cell targeting through pH modulation, Commun Biol 1 (1) (2018) 48, https://doi.org/10.1038/s42003-018-0047-1.
[18] G.H. Bardy, F. Coltorti, T.D. Ivey, et al., Some factors affecting bubble formation with catheter-mediated defibrillator pulses, Circulation 73 (3) (1986) 525–538, https://doi.org/10.1161/01.CIR.73.3.525.
[19] Saulis G, Rodaitė-Riševičienė R, Saulė R. Cytotoxicity of a Cell Culture Medium Treated with a High-Voltage Pulse Using Stainless Steel Electrodes and the Role of Iron Ions. Membranes (Basel) 2022; 12(2):184; doi: 10.3390/membranes12020184.
[20] R. Stapulionis, Electric pulse-induced precipitation of biological macromolecules in electroporation, Bioelectrochem Bioenerg 48 (1) (1999) 249–254, https://doi.org/10.1016/s0302-4598(98)00206-2.
[21] B. Roodenburg, J. Morren, H.E.I. Berg, S.W.H. de Haan, Metal release in a stainless steel pulsed electric field (PEF) system: Part II. The treatment of orange juice; related to legislation and treatment chamber lifetime, Innov. Food Sci. Emerg. Technol. 6 (3) (2005) 337–345, https://doi.org/10.1016/j.ifset.2005.04.004.
[22] S. Mahnič-Kalamiza, D. Miklavčič, P. Lombergar, et al., Elucidating the mechanisms of microbubble formation in intracardiac pulsed field ablation, Electrochim. Acta 497 (2024) 144550, https://doi.org/10.1016/j.electacta.2024.144550.
[23] B.E.W. Nordenstrom, Preliminary clinical trials of electrophoretic ionization in the treatement of malignant tumors, IRCS Medical Sc. 6 (1978) 537–540.
[24] M.K. Stehling, E. Guenther, P. Mikus, et al., Synergistic Combination of Electrolysis and Electroporation for Tissue Ablation, PLoS One 11 (2) (2016) e0148317, https://doi.org/10.1371/journal.pone.0148317.
[25] N. Klein, E. Guenther, F. Botea, et al., The combination of electroporation and electrolysis (E2) employing different electrode arrays for ablation of large tissue volumes, PLoS One 14 (8) (2019) e0221393, https://doi.org/10.1371/journal.pone.0221393.
[26] Y. Lv, C. Yao, B. Rubinsky, A 2-D cell layer study on synergistic combinations of high-voltage and low-voltage irreversible electroporation pulses, IEEE Trans. Biomed. Eng. 67 (4) (2020) 957–965, https://doi.org/10.1109/TBME.2019.2925774.
[27] N. Klein, B. Mercadal, M. Stehling, A. Ivorra, In vitro study on the mechanisms of action of electrolytic electroporation (E2), Bioelectrochemistry 133 (2020) 107482, https://doi.org/10.1016/j.bioelechem.2020.107482.
[28] H.B. Kim, J.H. Chung, Incorporation of reversible electroporation into electrolysis accelerates apoptosis for rat liver tissue, Technol Cancer Res Treat. 19 (2020) 1533033820948051, https://doi.org/10.1177/1533033820948051.
[29] M. Valko, H. Morris, M.T. Cronin, Metals, toxicity and oxidative stress, Curr Med Chem. 12 (10) (2005) 1161–1208, https://doi.org/10.2174/0929867053764635. PMID: 15892631.
[30] G. Saulis, R. Lape, R. Praneviciūte, D. Mickevicius, Changes of the solution pH due to exposure by high-voltage electric pulses, Bioelectrochemistry 67 (1) (2005) 101–108, https://doi.org/10.1016/j.bioelechem.2005.03.001.
[31] A. Tesse, F.M. André, T. Ragot, Aluminum particles generated during millisecond electric pulse application enhance adenovirus-mediated gene transfer in L929 cells, Sci Rep. 11 (1) (2021) 17725, https://doi.org/10.1038/s41598-021-96781-y.
[32] A. Vižintin, S. Marković, J. Ščančar, D. Miklavčič, Electroporation with nanosecond pulses and bleomycin or cisplatin results in efficient cell kill and low metal release from electrodes, Bioelectrochemistry 140 (2021) 107798, https://doi.org/10.1016/j.bioelechem.2021.107798.
[33] H. Chen, Y. Tang, Iron-loaded extracellular vesicles: angel or demon? Free Radic Res. 57 (1) (2023) 61–68, https://doi.org/10.1080/10715762.2023.2191813.
[34] C.W. Brown, J.J. Amante, P. Chhoy, et al., Prominin2 drives ferroptosis resistance by stimulating iron export, Dev Cell. 51 (5) (2019) 575–586.e4, https://doi.org/10.1016/j.devcel.2019.10.007.
[35] M. Riegman, L. Sagie, C. Galed, et al., Ferroptosis occurs through an osmotic mechanism and propagates independently of cell rupture, Nat Cell Biol. 22 (9) (2020) 1042–1048, https://doi.org/10.1038/s41556-020-0565-1.
[36] J. Wu, Z. Li, Y. Wu, N. Cui, The crosstalk between exosomes and ferroptosis: a review, Cell Death Discov. 10 (1) (2024) 170, https://doi.org/10.1038/s41420-024-01938-z.
[37] A.A. Baxter, Stoking the fire: How dying cells propagate inflammatory signalling through extracellular vesicle trafficking, Int J Mol Sci. 21 (19) (2020) 7256, https://doi.org/10.3390/ijms21197256.
[38] M. Xiong, Z. Chen, J. Tian, Y. Peng, D. Song, L. Zhang, Y. Jin, Exosomes derived from programmed cell death: mechanism and biological significance, Cell Commun Signal. 22 (1) (2024) 156, https://doi.org/10.1186/s12964-024-01521-0.
[39] A. Costigan, E. Hollville, S.J. Martin, Discriminating between apoptosis, necrosis, necroptosis, and ferroptosis by microscopy and flow cytometry, Curr Protoc. 3 (12) (2023) e951.
[40] A.G. Levis, F. Majone, Cytotoxic and clastogenic effects of soluble chromium compounds on mammalian cell cultures, Br J Cancer. 40 (4) (1979) 523–533, https://doi.org/10.1038/bjc.1979.217.
[41] F.W. Sunderman Jr., Mechanisms of nickel carcinogenesis, Scand J Work Environ Health. 15 (1) (1989) 1–12, https://doi.org/10.5271/sjweh.1888.
[42] G.G. Fletcher, F.E. Rossetto, J.D. Turnbull, E. Nieboer, Toxicity, uptake, and mutagenicity of particulate and soluble nickel compounds, Environ Health Perspect. 102 Suppl 3(Suppl 3) (1994) 69–79, https://doi.org/10.1289/ehp.94102s369.
[43] C.A. Grillo, M.A. Reigosa, M.F. Lorenzo de Mele, Effects of copper ions released from metallic copper on CHO-K1 cells, Mutat Res. 672 (1) (2009) 45–50, https://doi.org/10.1016/j.mrgentox.2008.09.012.
[44] W. Szlasa, A. Kiełbik, A. Szewczyk, et al., Oxidative effects during irreversible electroporation of melanoma cells-in vitro study, Molecules 26 (1) (2020) 154, https://doi.org/10.3390/molecules26010154.
[45] K. Balantič, V.U. Weiss, E. Pittenauer, et al., The role of lipid oxidation on electrical properties of planar lipid bilayers and its importance for understanding electroporation, Bioelectrochemistry 153 (2023) 108498, https://doi.org/10.1016/j.bioelechem.2023.108498.
[46] Y. Lv, C. Yao, B. Rubinsky, A conceivable mechanism responsible for the synergy of high and low voltage irreversible electroporation pulses, Ann Biomed Eng. 47 (7) (2019) 1552–1563, https://doi.org/10.1007/s10439-019-02258-5.
[47] R. Šmerc, D. Miklavčič, S. Mahnič-Kalamiza, An experimentally validated numerical model for pH changes in surrogate tissue induced by electroporation pulses, Electrochim. Acta (2024) 145363, https://doi.org/10.1016/j.electacta.2024.145363.
[48] M.P. Ryan, D.E. Williams, R.J. Chater, et al., Why stainless steel corrodes, Nature 415 (6873) (2002) 770–774, https://doi.org/10.1038/415770a.
[49] G. Tranchida, M. Clesi, F. Di Franco, et al., Electronic properties and corrosion resistance of passive films on austenitic and duplex stainless steels, Electrochim. Acta 273 (2018) 412–423, https://doi.org/10.1016/j.electacta.2018.04.058.
[50] C. Örnek, B. Payam, A. Gloskovskii, et al., Understanding the passive behaviour of low-chromium high-strength Hybrid steel in corrosive environments, Npj Mater Degrad. 7 (2023) 71, https://doi.org/10.1038/s41529-023-00392-z.
[51] Y. Hedberg, X. Wang, J. Hedberg, et al., Surface-protein interactions on different stainless steel grades: effects of protein adsorption, surface changes and metal release, J Mater Sci Mater Med. 24 (4) (2013) 1015–1033, https://doi.org/10.1007/s10856-013-4859-8.
[52] Maurice V, Yang WP, Marcus P. X-ray photoelectron spectroscopy and scanning tunneling microscopy study of passive films formed on (100) Fe-18Cr-13Ni single-crystal surfaces. J. Electrochem. Soc. 1998; 145:909; doi: 10.1149/1.1838366.
[53] M. Kovendhan, H. Kang, S. Jeong, et al., Study of stainless steel electrodes after electrochemical analysis in sea water condition, Environ Res. 173 (2019) 549–555, https://doi.org/10.1016/j.envres.2019.03.069.
[54] W. Xu, F. Yu, L. Yang, et al., Accelerated corrosion of 316L stainless steel in simulated body fluids in the presence of H2O2 and albumin, Mater. Sci. Eng. C, Biomimetic Mater. Sensors Syst. 11–19 (2018) doi:101016/jmsec201806023.
[55] Y.C. Tang, S. Katsuma, S. Fujimoto, S. Hiromoto, Electrochemical study of Type 304 and 316L stainless steels in simulated body fluids and cell cultures, Acta Biomater. 2 (6) (2006) 709–715, https://doi.org/10.1016/j.actbio.2006.06.003.
[56] M. Långberg, C. Örnek, J. Evertsson, et al., Redefining passivity breakdown of super duplex stainless steel by electrochemical operando synchrotron near surface X-ray analyses, Npj Mater Degrad. 3 (2019) 22, https://doi.org/10.1038/s41529-019-0084-3.
[57] S.E. Fendorf, G. Li, Kinetics of chromate reduction by ferrous iron, Environ. Sci. Technol. 30 (5) (1996) 1614–1617, https://doi.org/10.1021/es950618m.
[58] G. Song, Transpassivation of Fe–Cr–Ni stainless steels, Corros. Sci. 47 (8) (2005) 1953–1987, https://doi.org/10.1016/j.corsci.2004.09.007.
[59] V. Maurice, P. Marcus, Progress in corrosion science at atomic and nanometric scales, Prog. Mater Sci. 95 (2018) 132–171, https://doi.org/10.1016/j.pmatsci.2018.03.001.
[60] I. Betova, M. Bojinov, T. Laitinen, et al., The transpassive dissolution mechanism of highly alloyed stainless steels: I. Experimental results and modelling procedure, Corros. Sci. 44 (12) (2002) 2675–2697, https://doi.org/10.1016/S0010-938X(02)00073-2.
[61] P. Sharma, S.P. Singh, S.K. Parakh, Y.W. Tong, Health hazards of hexavalent chromium (Cr (VI)) and its microbial reduction, Bioengineered. 13 (3) (2022) 4923–4938, https://doi.org/10.1080/21655979.2022.2037273.
[62] A. Muñoz, M. Costa, Elucidating the mechanisms of nickel compound uptake: a review of particulate and nano-nickel endocytosis and toxicity, Toxicol Appl Pharmacol. 260 (1) (2012) 1–16, https://doi.org/10.1016/j.taap.2011.12.014.
[63] A. Chiu, X.L. Shi, W.K. Lee, et al., Review of chromium (VI) apoptosis, cell-cycle-arrest, and carcinogenesis, J Environ Sci Health C Environ Carcinog Ecotoxicol Rev. 28 (3) (2010) 188–230, https://doi.org/10.1080/10590501.2010.504980.
[64] F. Vana, Z. Szabo, M. Masarik, M. Kratochvilova, The interplay of transition metals in ferroptosis and pyroptosis, Cell Div 19 (1) (2024) 24, https://doi.org/10.1186/s13008-024-00127-9.

[65] K. Honarmand Ebrahimi, P.L. Hagedoorn, W.R. Hagen, Unity in the biochemistry of the iron-storage proteins ferritin and bacterioferritin, Chem Rev. 115 (1) (2015) 295–326, https://doi.org/10.1021/cr5004908.
[66] D.M. Ward, J. Kaplan, Ferroportin-mediated iron transport: expression and regulation, Biochim Biophys Acta. 1823 (9) (2012) 1426–1433, https://doi.org/10.1016/j.bbamcr.2012.03.004.
[67] M. Truman-Rosentsvit, D. Berenbaum, L. Spektor, et al., Ferritin is secreted via 2 distinct nonclassical vesicular pathways, Blood 131 (3) (2018) 342–352, https://doi.org/10.1182/blood-2017-02-768580.
[68] A. Alur, J. Phillips, D. Xu, Effects of hexavalent chromium on mitochondria and their implications in carcinogenesis, J. Environ. Sci. Health C 42 (2) (2024) 109–125, https://doi.org/10.1080/26896583.2024.2301899.
[69] K.C. Edwards, M.W. Gannon, P.A. Frantom, J.B. Vincent, Low-molecular-weight chromium-binding substance (LMWCr) may bind and carry Cr(III) from the endosome, J Inorg Biochem. 223 (2021) 111555, https://doi.org/10.1016/j.jinorgbio.2021.111555.
[70] D.R. Graham, E. Drummond, M. Barrido, J.B. Vincent, Binding Chromium(III) to Form Mixed Cr(III),Fe(III) Serum Transferrins, Biol Trace Elem Res. 202 (7) (2024) 3377–3382, https://doi.org/10.1007/s12011-023-03917-4.
[71] M. Gao, J. Yi, J. Zhu, A.M. Minikes, P. Monian, C.B. Thompson, X. Jiang, Role of Mitochondria in Ferroptosis, Mol Cell. 73 (2) (2019) 354–363.e3, https://doi.org/10.1016/j.molcel.2018.10.042.
[72] S. Terpilowska, A.K. Siwicki, Cell cycle and transmembrane mitochondrial potential analysis after treatment with chromium(iii), iron(iii), molybdenum(iii) or nickel(ii) and their mixtures, Toxicol Res (camb). 8 (2) (2018) 188–195, https://doi.org/10.1039/c8tx00233a.
[73] Y.J. Lee, S.S. Lim, B.J. Baek, et al., Nickel(II)-induced nasal epithelial toxicity and oxidative mitochondrial damage, Environ Toxicol Pharmacol. 42 (2016) 76–84, https://doi.org/10.1016/j.etap.2016.01.005.
[74] M.B. Kastan, D.S. Lim, The many substrates and functions of ATM, Nat Rev Mol Cell Biol. 1 (3) (2000) 179–186, https://doi.org/10.1038/35043058.
[75] M. Marcussen, P.J. Larsen, Cell cycle-dependent regulation of cellular ATP concentration, and depolymerization of the interphase microtubular network induced by elevated cellular ATP concentration in whole fibroblasts, Cell Motil Cytoskeleton. 35 (2) (1996) 94–99, https://doi.org/10.1002/(SICI)1097-0169(1996)35:2<94::AID-CM2>3.0.CO;2-I.
[76] M.J. da Veiga, S. Peres, J.M. Steyaert, et al., Cell cycle progression is regulated by intertwined redox oscillators, Theor Biol Med Model. 12 (2015) 10, https://doi.org/10.1186/s12976-015-0005-2.
[77] A.R. Khaled, D.A. Reynolds, H.A. Young, et al., Interleukin-3 withdrawal induces an early increase in mitochondrial membrane potential unrelated to the Bcl-2 family. Roles of intracellular pH, ADP transport, and F(0)F(1)-ATPase, J Biol Chem. 276 (9) (2001) 6453–6462, https://doi.org/10.1074/jbc.M006391200.
[78] P. Neupane, S. Bhuju, N. Thapa, H.K. Bhattarai, ATP Synthase: Structure, Function and Inhibition. Biomol Concepts. 10 (1) (2019) 1–10, https://doi.org/10.1515/bmc-2019-0001.
[79] Y. Ouyang, M.Y. Jeong, C.N. Cunningham, et al., Phosphate starvation signaling increases mitochondrial membrane potential through respiration-independent mechanisms, Elife 13 (2024) e84282, https://doi.org/10.7554/eLife.84282.
[80] S. Li, Y. Zhou, Q. Huang, et al., Iron overload in endometriosis peritoneal fluid induces early embryo ferroptosis mediated by HMOX1, Cell Death Discov. 7 (1) (2021) 355, https://doi.org/10.1038/s41420-021-00751-2.
[81] A. Perl, P. Gergely Jr, G. Nagy, et al., Mitochondrial hyperpolarization: a checkpoint of T-cell life, death and autoimmunity, Trends Immunol. 25 (7) (2004) 360–367, https://doi.org/10.1016/j.it.2004.05.001.
[82] V.P. Skulachev, Mitochondrial physiology and pathology; concepts of programmed death of organelles, cells and organisms, Mol Aspects Med. 20 (3) (1999) 139–184, https://doi.org/10.1016/s0098-2997(99)00008-4.
[83] L.D. Zorova, V.A. Popkov, E.Y. Plotnikov, et al., Mitochondrial membrane potential, Anal Biochem. 552 (2018) 50–59, https://doi.org/10.1016/j.ab.2017.07.009.
[84] T. Polajžer, W. Peng, C. Yao, D. Miklavčič, Changes in Mitochondrial Membrane Potential in In Vitro Electroporation with Nano- and Microsecond Pulses, Bioelectricity. 6 (2) (2024) 97–107, https://doi.org/10.1089/bioe.2024.0007.